Materials Science & Engineering C 100 (2019) 897–914

Contents lists available at ScienceDirect

Materials Science & Engineering C

journal homepage: www.elsevier.com/locate/msec

Synthesis, characterization, and utilization of a diallylmethylamine-based cyclopolymer for corrosion mitigation in simulated acidizing environment

Saviour A. Umoren[a,*], Moses M. Solomon[a], Shaikh A. Ali[b], Hatim D.M. Dafalla[c]

[a] Centre for Research Excellence in Corrosion, Research Institute, King Fahd University of Petroleum and Minerals, Dhahran 31261, Saudi Arabia
[b] Department of Chemistry, Faculty of Science, King Fahd University of Petroleum and Minerals, Dhahran 31261, Saudi Arabia
[c] Centre for Engineering Research, Research Institute, King Fahd University of Petroleum and Minerals, Dhahran 31261, Saudi Arabia

ARTICLE INFO

Keywords:
Synthesis
Copolymer
Acid corrosion
Corrosion inhibition
Adsorption
Synergism

ABSTRACT

A novel random copolymer **4**, containing diallylmethylamine and N^1,N^1-diallyl-N^1-methyl-N^6,N^6,N^6-tripropylhexane-1,6-diammonium dibromide units in a 1:1 ratio (polymer **4**) was synthesized via Butler's cyclopolymerization technique. Characterization was accomplished by ^{1}H NMR, elemental analysis, and Fourier-transform infrared spectroscopy (FTIR). Polymer **4** was tested as corrosion inhibitor for low carbon steel in 15% HCl solution via gravimetric and electrochemical approaches. The analysis of the metal specimen surfaces was done using scanning electron microscope (SEM), atomic force microscopy (AFM), energy dispersive X-ray spectroscopy (EDAX), and X-ray photoelectron spectroscopy (XPS) methods. Polymer **4** is inhibitor for the substrate particularly at elevated temperatures. Corrosion mitigation is by chemisorption mechanism and can be best described with the Langmuir and El-Awady et al. kinetic-thermodynamic adsorption isotherms. Polymer **4** corrosion mitigation capacity can be improved by the addition of a minute amount of I^- ions. Inhibition efficiency of 92.99% has been achieved with 500 ppm polymer **4** + 1 mM KI mixture at 25 °C. Surface analysis results support the claim of adsorption of additive molecules on steel surface. From XPS results, corrosion products on steel surface exposed to the free acid solution are mixtures of chlorides, carbonates, oxides, and hydroxides. In polymer **4** + KI system, polymer **4** molecules are adsorbed on triiodide and pentaiodide ions layer. The improved corrosion inhibition of polymer **4** by I^- ions is synergistic in nature according to calculated synergism parameter. Polymer **4** is a promising corrosion inhibitor for oil well acidizing purpose.

1. Introduction

One of the sectors driving the global economy is the oil and gas exploration and production industry. Currently, the sector contributes 2–3% to the global economy with a total revenue of 2 trillion USD [1]. Acidizing is a widely used production stimulation strategy in new and aging wells [2,3]. Concentrated acid solution mostly HCl or HCl/HF mixture is pumped under pressure into wellbore to dissolve rock formation or to create new flow path [2,3]. Corrosion of well tubulars (mostly low carbon steel) is aggravated as acid solution gets in contact. As a matter of necessity, the acid solution is fortified with effective corrosion inhibitors. Organic compounds, particularly nitrogen containing compounds have been claimed to possess anticorrosive property in acidizing environment. For example, Engle and Keeney [4] in the US Patent No. 3,514,410 claimed that, with 0.3% Rodine 213, an inhibitor formulation containing a rosin amine, a formaldehyde, and a ketone, corrosion rate of 0.089 lbs./ft.^{2}/24 h can be achieved. In the US Patent No. 3,404,094, Keeney [5] disclosed that inhibitor formulation consisting of an amine or nitrogen-based compound, acetylenic alcohol, and a non-acetylenic alcohol was capable of restricting A-110 steel corrosion to a rate in the range 0.033–0.156 lbs./ft^2/24 h at temperature of 150–175 °C. Similar claims can be found in the US Patent Nos. 3,107,221 [6] and 2,993,863 [7]. Although these formulations are effective acid corrosion inhibitors, the toxicity of some of the components like acetylenic alcohol would limit their applications as the campaign for greenness intensifies.

In the last few years, research light has beamed on polymeric materials, both natural and synthetic for utilization as metals corrosion inhibitors in diverse aggressive media [8–11]. Comprehensive information on polymeric corrosion inhibitors for the oil and gas industry can be found in the report by Tiu and Advincula [12]. Polymers are environmentally friendly, possess inherent stability, and have multiple adsorption centers. However, in some cases, polymers exhibit moderate corrosion inhibiting performance [13,14] as a result of their poor

* Corresponding author.
E-mail address: umoren@kfupm.edu.sa (S.A. Umoren).

https://doi.org/10.1016/j.msec.2019.03.057
Received 21 October 2018; Received in revised form 17 February 2019; Accepted 17 March 2019
Available online 21 March 2019

solubility property in aqueous medium. Some reports have highlighted the enhancement of the corrosion inhibition efficiency of polymeric compounds by combination with metals cations [15–18] or halide anions [19–22]. In our laboratory, we have equally demonstrated the beneficial influence of halide ions particularly iodide ions on protection effectiveness of polymers [23,24].

In a quest to continue to develop polymer-based corrosion inhibitors for industrial application, poly(DAMA-*ran*-DAMTDB) **4** was synthesized. In this communication, we present the synthesis and use of poly (DAMA-*ran*-DAMTDB) **4**, where DAMA and DAMTDB stand for diallylmethylamine and N^1,N^1-diallyl-N^1-methyl-N^6,N^6,N^6-tripropylhexane-1,6-diammonium dibromide, respectively, with iodide ions as a highly potent corrosion suppressor for low carbon steel in acidizing medium. Poly(DAMA-*ran*-DAMTDB) **4**, which onwards will also be referred to as polymer **4**, synthesized from inexpensive starting materials, was characterized using ^{1}H NMR spectroscopy and the anticorrosion studies was done using weight loss, electrochemical, and surface analysis techniques. Note that the presence of corrosion inhibition motifs of trivalent amine, quaternary ammonium, hydrophobic alkyl spacers, and the multiple anchoring points provided by the polymer chain of **4** are all points towards an exciting outcome of the current study.

2. Experimental section

2.1. Synthesis of polymer 4

The synthesis route of the polymer **4** is illustrated in Scheme 1.

Amine **1** was prepared by reacting formic acid, diallylamine and paraformaldehyde using procedure described in Clarke et al. [25].

Butler's cyclopolymerization protocol [26] was adopted for the polymerization of diallylmethylammonium chloride (DAMAC) (**1-HCl**) monomer. Thus, stirred amine **1** (5.0 g, 45 mmol) in a 100 mL RB flask fitted with a long condenser was neutralized with concentrated HCl (4.93 g, 37 wt%, 50 mmol) at 0 °C. The monomer solution was degassed with N_2 and then heated to 100 °C. Three portions of the initiator ammonium persulfate (APS) (3 × 0.25 g) was added at 3 min interval. The temperature of the exothermic reaction rose to 110 °C. The reaction mixture was continuously stirred at the oil bath temperature of 100 °C for an additional 20 min. The reaction mixture was then dialyzed against distilled water (3 h) and freeze-dried to obtain poly(DAMAC) **2** (5.5 g, 83%) as a hygroscopic white powder. The intrinsic viscosities [η] of polymer **2** in 0.1 M NaCl at 30 °C was determined using an Ubbelohde viscometer (having a Viscometer Constant of 0.005718 cSt/s at all temperatures) and found to be 0.0785 dL g^{-1}. The low viscosity value indicates the lower molar mass of the polymer.

Bromide salt **3** was prepared using literature procedure [27]. Polymer **2** was transformed to **4** using procedure as described in Tian et al. [27]. Thus, powdered NaOH (0.8 g, 20 mmol) was added to a stirring solution of **2** (2.95 g, 20 mmol in terms of the repeating unit) in methanol (8 mL) under N_2. Toluene (40 mL), acetonitrile (40 mL), and **3** (4.94 g, 78.4% purity, 10 mmol) were added to the cloudy mixture and the contents in the closed reaction flask was heated at 70 °C for 20 h under N_2. After the removal of the solvents, the mixture was dialyzed in the presence of excess KBr to obtain poly(DAMA-*ran*-DAMTDB) **4** in 88% yield.

2.2. Characterization of poly(DAMA-ran-DAMTDB) 4

A Bruker 500 MHz instrument operating at 500 MHz was used for ^{1}H NMR characterization of polymer **4** in D_2O.

2.3. Anticorrosion studies

2.3.1. Materials/solutions preparation

Steel specimens were cut out of a sheet of St37–2 steel grade purchased from Erdemir Steel Co., Turkey. The chemical composition of the steel grade is as given in Solomon et al. [11]. The dimension of the samples used for weight loss experiments was 3.0 × 3.0 cm × 0.2 cm. The surface area was calculated using Eq. (1) [28]. Samples for electrochemical experiments were circular in shape with 0.79 cm^2 as the surface area. All the specimens were subjected to mechanical abrasion using silicon carbide paper of different grits. To get rid of the dust generated from the abrasion process, the samples were sonicated in ethanol bath for ten minutes, degreased with ethanol and acetone, and then dried using Buehler Torramet specimen dryer. The corrodent was 15% HCl solution prepared by diluting concentrated hydrochloric acid (37%) with distilled water. The concentration of polymer **4** studied was 50, 100, 300, 500, and 700 ppm while the concentration of KI used was 0.001 M. It is worth mentioning that polymer **4** is a water-soluble polymer and did not require special organic solvent for dissolution.

$$A = 2(wl + dl + dw) \quad (1)$$

where A = area (cm^2); w = width (cm); d = thickness (cm); and l = length (cm).

2.3.2. Weight loss experiments

The gravimetric experiments were performed following the ASTM standard procedure [28]. Firstly, the initial weight of the coupons was measured using a digital weighing balance of precision ± 0.1 mg and the weight was designated as W_0. Secondly, reaction bottles which were properly labeled were filled with 100 mL of the respective test solutions. Thirdly, two pre-weighed St37–2 steel samples were freely suspended in each of the reaction bottles. The reaction vessels were placed in a thermostatic water bath maintained at studied temperature for 6 h. Fourthly, the corroded samples were retrieved after 6 h of immersion, immersed in 1 M HCl for 20 s to loosen the corrosion deposits [29], washed in distilled water, rinsed in acetone, and finally dried using Buehler Torramet specimen dryer. The dried metal specimens were reweighed and the new weight designated as W_1. The weight loss (WL) was computed thus:

$$WL\ (g) = W_0 - W_1 \quad (2)$$

To determine the corrosion rate (v), the mean weight loss ($\overline{WL}$, g) was used following Eq. (3) [30]:

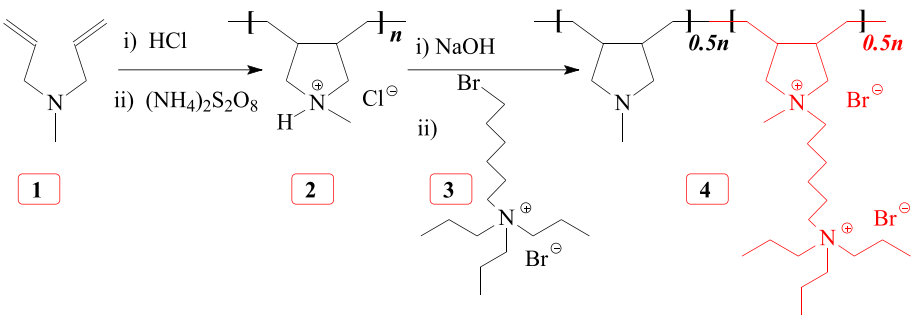

Scheme 1. Synthesis of polymeric inhibitor 4.

$$v(\text{mm/yr}) = \frac{87600 \times \overline{WL}}{\rho AT} \quad (3)$$

where ρ = density of the steel sample (g cm^{-3}), T = immersion time (h), and A = surface area of the specimen (cm^2).

The inhibition efficiency (η, %) of polymer **4** was calculated using Eq. (4):

$$\eta(\%) = \frac{v(\text{blank}) - v(\text{inh.})}{v(\text{blank})} \times 100 \quad (4)$$

where $v_{(\text{blank})}$ = corrosion rate in the blank solution and $v_{(\text{inh.})}$ = corrosion rate in the corrodent containing polymer **4**.

2.3.3. Electrochemical measurements

The electrochemical experiments were performed in accordance with the ASTM G3-89 [31] and G5-94 [32] standards. An electrochemical workstation, Gamry Potentiostat/galvanost/ZRA (Ref 600) which has EIS300, EFM 140, and DC105 softwares for impedance, intermodulation, and polarization measurements respectively was used for the electrochemical studies. The electrochemical cell was a tri-electrode component type whereby the prepared metal specimen serves as the working electrode, Ag/AgCl as the reference electrode, and a graphite rod as the counter electrode. Prior to electrochemical measurements, the working electrode was allowed to stand in test solution for 3600 s for the purpose of ensuring a steady state open-circuit potential (OCP). For the electrochemical impedance spectroscopy measurements, the experimental setup was as follows: initial frequency = 100, 000 Hz, final frequency = 0.01 Hz, amplitude = 10 mV peak to peak. The impedance obtained were analyzed using Gamry Echem Analyst. For potentiodynamic polarization (PDP) measurements, the initial potential was – 0.25 V vs. open circuit potential (E_{ocp}) and the final potential was 0.25 V vs. E_{ocp} while the scan rate was 0.2 mV/s. An extrapolation method was used to derive the polarization parameters such as E_{corr}, current density (i_{corr}), anodic and cathodic Tafel slopes (β_a & β_c), etc. from the obtained polarization curves. Electrochemical frequency modulation (EFM) experiments were carried out setting the base frequency at 1 Hz and number of cycles at 32 such that the sinusoidal waveform repeats after 1 s. The amplitude of perturbation was 10 mV and 2 and 5 Hz were the measurements frequencies. Linear polarization resistance (LPR) testing were realized by polarizing the working electrode from initial potential of −0.01 V vs. E_{ocp} to the final potential of +0.01 V vs. E_{ocp} at a sweep rate of 0.125 mV/s. The polarization resistance (R_p) was obtained from the slope of the potential-current graph in the vicinity of E_{corr}. The inhibition efficiency (η) from electrochemical impedance spectroscopy (EIS) was calculated using Eq. (5). η from PDP and EFM was computed using Eq. (6) while the η values from LPR was calculated making use of Eq. (7).

$$\eta_{\text{EIS}} = \left(1 - \frac{R^0}{R}\right) \times 100 \quad (5)$$

$$\eta_{\text{PDP}} = \left(1 - \frac{i_{\text{corr}}}{i^0_{\text{corr}}}\right) \times 100 \quad (6)$$

$$\eta_{\text{LPR}} = \left(1 - \frac{R^0_p}{R_p}\right) \times 100 \quad (7)$$

where R^0,$i_{\text{corr}}{}^0$, and $R_p{}^0$, are the charge transfer resistance, corrosion current density, and polarization resistance respectively recorded in acid solution devoid of polymer **4**. R,i_{corr}, and R_p are the charge transfer resistance, corrosion current density, and polarization resistance respectively in the presence of polymer **4**.

2.3.4. Surface examination

The surface properties of the steel samples exposed to the studied acid environment in the absence and presence of polymer **4** for 24 h and the elemental composition of the corrosion deposits and/or adsorbed polymer **4** films on the sample surfaces were determined with the help of a Scanning Electron Microscope (SEM) JEOL JSM-6610 LV coupled to energy dispersive X-ray spectroscopy (EDAX). The SEM instrument was accelerated at 20 kV. The degree of roughness of the studied metal surfaces were assessed using 5420 atomic force microscope (N9498S, Agilent Technologies, UK) operated in the contact mode under ordinary conditions. X-ray photoelectron spectroscopy (XPS) analysis was undertaken using a ESCALAB 250Xi XPS spectrometer with a monochromatic Al Kα X-ray source. The data were obtained from the specimen surface directly without Ar ion sputtering. Analysis of the XPS data was done using Avantage v5,51,0,5371 software. However, the preparation procedure of samples for SEM-EDAX, XPS, and AFM analysis was different. For AFM analysis, the samples after removing from test solutions were gently washed under running water, rinsed with acetone, and dried with sample dryer before subjecting to the analysis. The cleaning process was avoided in samples used for SEM, EDAX, and XPS analysis; reason being that, our interest was on the adsorbed film.

3. Results and discussion

3.1. NMR, FTIR, and elemental analyses

Polymer **4** was characterized using ^{1}H NMR, FTIR spectroscopy and elemental analysis; the spectra obtained are presented in Fig. 1. From the characterization, the following was found: C, 56.7; H, 10.0; N, 6.7%. Polymer **4** with a 1:1 copolymer composition requires C, 57.14; H, 9.76; N, 6.89%); ν_{max}. (KBr) 3437, 2931, 2859, 2782, 1641, 1471, 1388, 1129, 1045, 960, 758, and 620 cm^{-1}. FTIR peaks found: 3403.93, 2931.99, 2873.84, 2770.36, 1661.65, 1455.86, 1385.95,

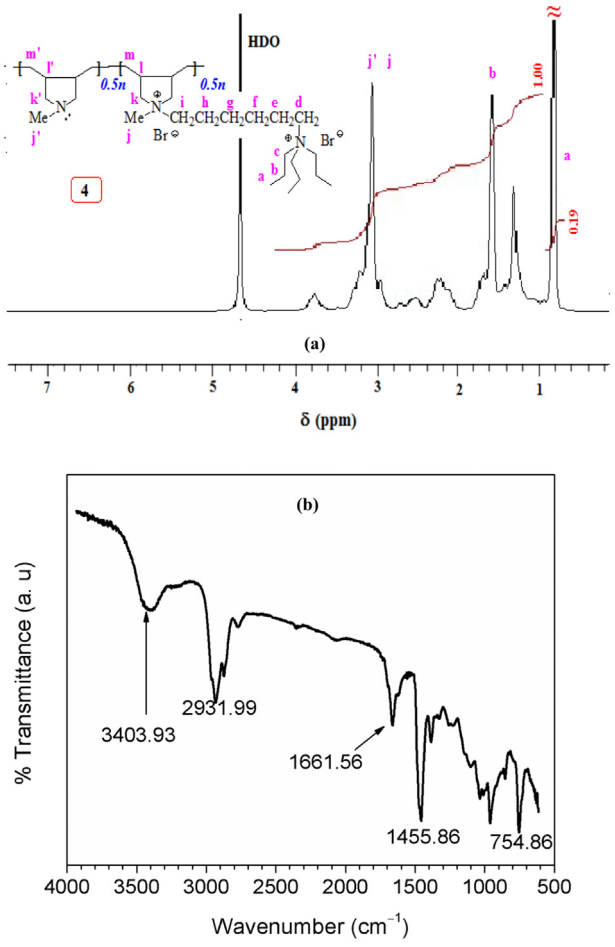

Fig. 1. (a) ^{1}H NMR and (b) FTIR spectra of polymer **4**.

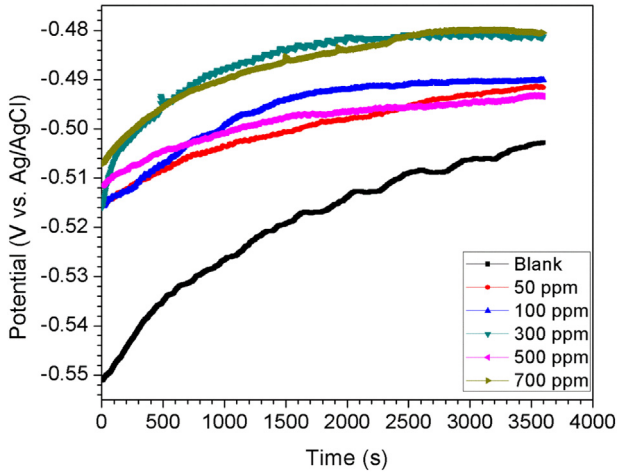

Fig. 2. Open circuit potential variations with time for St37–2 steel in 15% HCl solution without and with different concentrations of polymer **4** at 25 °C.

1035.50, 961.69, 835.76, and 754.68 cm^{-1}. The N—H of the tertiary amine and the ring C—N stretching are seen at 3403.93 cm^{-1} and 1035.50 cm^{-1} respectively. The extent of alkylation according to the elemental analysis was 50 mol%. The ^{1}H NMR and the FTIR results confirm the successful synthesis of polymer **4**.

3.2. OCP and EIS studies

To ensure a steady state condition before impedance and polarization measurements, the variation of open circuit potential (OCP) for St37–2 steel electrode in 15% HCl solution devoid of and containing various concentrations of polymer **4** was monitored for 3600 s. The results are displayed in Fig. 2. In acid solution free from polymer **4**, the initial OCP was – 0.5511 V vs. Ag/AgCl. The open potential steadily increased to – 0.5034 V vs. Ag/AgCl at 3479 s before attaining stability. This potential shift towards noble direction is associated with the formation of corrosion products on the steel electrode surface which offered partial protection against corrosion [33,34]. In comparison with the OCP vs. time graphs for the protected systems, the initial open potential of the protected systems is nobler than that of the unprotected and stability was attained in the inhibited acid solutions faster than in unprotected. For example, the initial OCP in acid solution inhibited with 50 ppm, 100 ppm, 300 ppm, 500 ppm, and 700 ppm polymer **4** is – 0.5155, – 0.5157, – 0.5159, – 0.5115, and – 0.5073 V vs. Ag/AgCl respectively and stability was attained at approximately 1500 s in all the systems. This observation is caused by the adsorption of polymer **4** molecules on the working electrode surface. Similar interpretation can be found in the corrosion literature [35–37].

Fig. 3 shows the electrochemical impedance spectra drawn for St37–2 steel in 15% HCl solution without and with various concentrations of polymer **4** in three formats: (a) Nyquist, (b) Bode modulus, and (c) Bode Phase. The Nyquist format (Fig. 3(a)) exhibits a common feature of a charge-controlled corrosion process, i.e. a single capacitive loop at high frequency region. The capacitive loop is far from being a perfect semicircle and is caused by the heterogeneous nature of the working electrode [35]. The capacitive loops drawn for inhibited systems are larger in size than that of uninhibited. This is indicative of slower charge transfer corrosion reactions in inhibited systems than in uninhibited. The concentration of inhibitor is found to have noticeable influence on the steel corrosion process. The size of the semicircle increases with increasing polymer **4** concentration up till 500 ppm and thereafter reduces. That is, the effect is in the order: 500 ppm > 700 ppm > 300 ppm > 100 ppm > 50 ppm. This effect is also seen in the Bode graphs (Fig. 3(b & c)) where the impedance modulus and the Phase angle are displayed towards bigger values in the afore listed

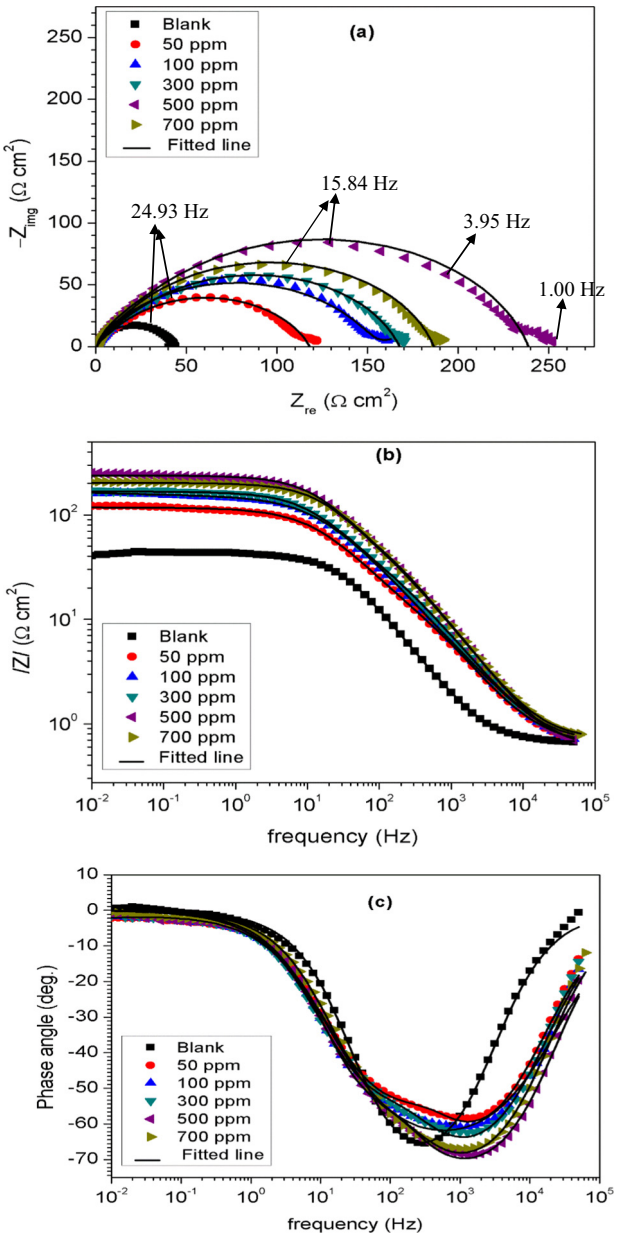

Fig. 3. Electrochemical impedance spectra for St37–2 steel in 15% HCl solution in the absence and presence of various concentrations of polymer **4** in (a) Nyquist and (b) Bode modulus representations at 25 °C.

order. The explanation is that, as the concentration of the inhibitor was increased, more inhibitor molecules were available for adsorption such that larger surface area was covered and many corrosion reaction sites blocked. The acid solution may have been saturated when 500 ppm polymer **4** was added such that further addition resulted in a scenario where adsorbed and un-adsorbed molecules interacted. Such interaction would cause the desorption of some of the adsorbed inhibitor molecules [38]. The 500 ppm concentration is therefore regarded as the optimum concentration of polymer **4**.

The analysis of the impedance data was done using a simple R(QR) circuit shown in Fig. 4(a). The equivalent circuit has the following elements, solution resistance (R_s), charge transfer resistance (R_{ct}), and constant phase element (CPE) which was imperative considering the deviation of the impedance from perfect semicircle. That is, the CPE represents the distorted double layer capacitance that was caused by the roughness of the working electrode surface. The equivalent circuit provided a good fit as evident from the fitted line in Fig. 3, the

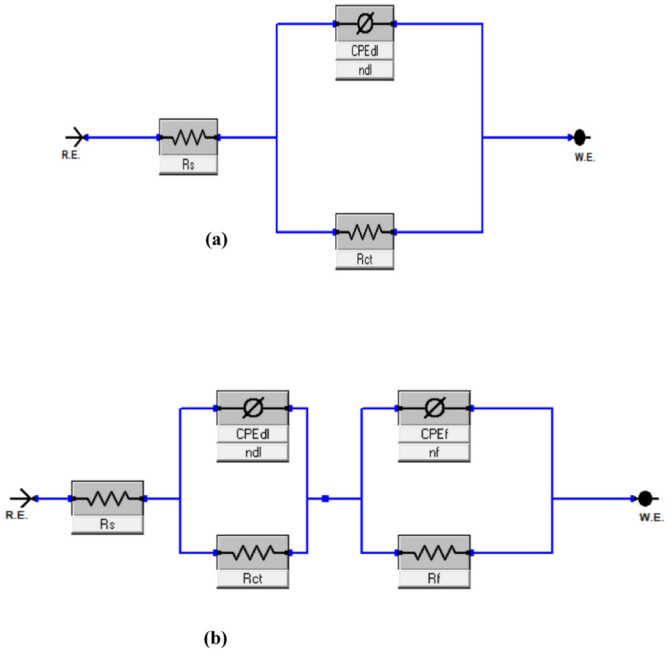

Fig. 4. Equivalent circuit diagrams used to fit (a) blank impedance data and (b) Polymer 4 and polymer **4** + KI data.

representative fitting images in Fig. S1 of the supporting information, and the small Chi squared and error values in Table 1. The CPE has two components, Y_0 (quantity of CPE) and n (phase shift parameter; $n = 2\alpha/(\pi)$) and these components were utilized in the calculation of the double layer capacitance (C_{dl}) of adsorbed film according to the following equation [39]:

$$C_{\mathrm{dl}} = (Y_0 R_{\mathrm{ct}}^{\mathrm{n}-1})^{1/\mathrm{n}} \quad (8)$$

The relaxation time constant (τ) of the charge-transfer process was calculated using Eq. (9) [40]:

$$\tau = C_{\mathrm{dl}} \times R_{\mathrm{ct}} \quad (9)$$

All the derived and calculated parameters are given in Table 1. From the results in the table, it is obvious that the R_{ct} value is higher and the C_{dl} value lower in the inhibited acid solutions than in uninhibited. The observed phenomenon is due to the adsorption and displacement of water molecules from the steel electrode surface by polymer **4** molecules [33,36]. According to Han et al. [36], the double layer capacitance of an electrode would decrease in the presence of inhibitor since the volume of water molecule is smaller and permittivity is higher than those of inhibitor molecule. The adsorbed polymer **4** films act as barrier layer posing stiff opposition to charge transfer as seen in Fig. 3(a). By inspecting Table 1 further, it is seen that upon increment of polymer **4** concentration from 50 ppm to 500 ppm, the R_{ct} value increased from 118.20 ± 0.65 Ω cm^2 to 236.80 ± 1.26 Ω cm^2 while the C_{dl} value decreased from 2.721 μF cm^{-2} to 2.150 μF cm^{-2}. A decrease in the local dielectric constant or increase in the thickness of adsorbed layer or both can give rise to the observed decrease in C_{dl} value with increasing inhibitor concentration according to the Helmholtz equation given elsewhere [33]. Considering the fact that the decline in C_{dl} value with increasing inhibitor concentration to 500 ppm is accompanied with increase in R_{ct} value and inhibition efficiency, it is reasonable to submit that increase in the thickness of adsorbed protective film was responsible for the observed decrease. The highest inhibition efficiency from the EIS technique achieved with the optimum concentration is 82.19%.

Further inspection of the results in Table 1 reveals that, after the addition of polymer **4** in the corrosive solution, the n increased from 0.73 in the 50 ppm polymer **4** inhibited solution to 0.80 in the 700 ppm polymer **4** containing solution. This behaviour can be associated with a decrease in the heterogeneity of the metal surface due to the adsorption of the inhibitor [40,41]. It is also observed from the table that the relaxation time constant (τ) increased from 0.0022 s in the blank solution to 0.0007 s in the acid solution inhibited with 700 ppm polymer **4**. Similar observation had been reported in the literature [40–43] and was interpreted to mean a decrease in the charge and discharge rates to the metal-solution interface. It indicates that there is agreement between the amount of charge that can be stored (i.e. capacitance) and the discharge velocity in the interface (τ) [40–43].

3.3. EFM, PDP, and LPR studies

The electrochemical frequency modulation (EFM) technique is becoming famous in the study of corrosion and corrosion inhibition. Its suitability in the assessment of specific forms of corrosion like crevice [44], pitting [45], and microbial influenced [46] corrosion had been determined. Obot and Onyeachu [47] recently carried out a review on the recent practical applications of EFM in corrosion research. The attractive feature of EFM lies in the so-called causality factors which allow the validity of data to be ascertained. Theoretically, the value of causality factor – 2 (CF–2) and the causality factor – 3 (CF–3) is expected to be within 0–2 and 0–3 respectively [47]. Fig. 5 shows typical intermodulation spectra obtained for steel specimen in 15% HCl solution devoid of and containing diverse dosages of polymer **4** at 25 °C. In the spectra, two sets of bands are observed; the sharp and long bands and the clouded bands. The clouded bands represent the background noise signals while the sharp and long peaks are the harmonic and intermodulation peaks [48] which were used for the computation of the electrochemical parameters listed in Table 2. The CF–2 and CF–3 values given in Table 2 are within the theoretical range hence the experimental data should be considered valid. The corrosion current density (i_{corr}) was remarkably reduced from 928.00 μA cm^{-2} in the free acid solution to 261.00 μA cm^{-2} in the 50 ppm polymer **4** inhibited solution and this reduction corresponded to 71.88% corrosion inhibition. The least i_{corr} (125.50 μA cm^{-2}) and the highest inhibition efficiency (86.48%) was achieved with the optimum concentration (500 ppm). The trend of variation of inhibition efficiency with inhibitor concentration is in conformity with the one noted in Table 1.

Table 1
Electrochemical impedance parameters for St37–2 steel in 15% HCl solution in the absence and presence of different concentrations of polymer **4** at 25 °C.

Conc. (ppm)	R_s (Ω cm^2)	CPE		R_{ct} (Ω cm^2)	C_{dl} (μF cm^{-2})	τ (s)	$x^2 \times 10^{-3}$	η_{EIS}
		Y_0 (μΩ^{-1} s^2 cm^{-2})	n					
0	0.67 ± 0.05	267.50	0.88 ± 0.03	42.18 ± 0.22	52.415	0.0022	0.49	–
50	0.55 ± 0.09	314.00	0.73 ± 0.00	118.20 ± 0.65	2.721	0.0003	1.34	64.31
100	0.54 ± 0.10	230.80	0.75 ± 0.00	156.60 ± 0.86	2.630	0.0004	1.54	73.07
300	0.59 ± 0.10	201.60	0.75 ± 0.00	167.30 ± 0.91	2.151	0.0004	2.65	74.79
500	0.51 ± 0.10	105.80	0.78 ± 0.00	236.80 ± 1.26	2.150	0.0005	3.48	82.19
700	0.67 ± 0.09	133.80	0.80 ± 0.00	185.00 ± 0.98	3.909	0.0007	2.46	77.20

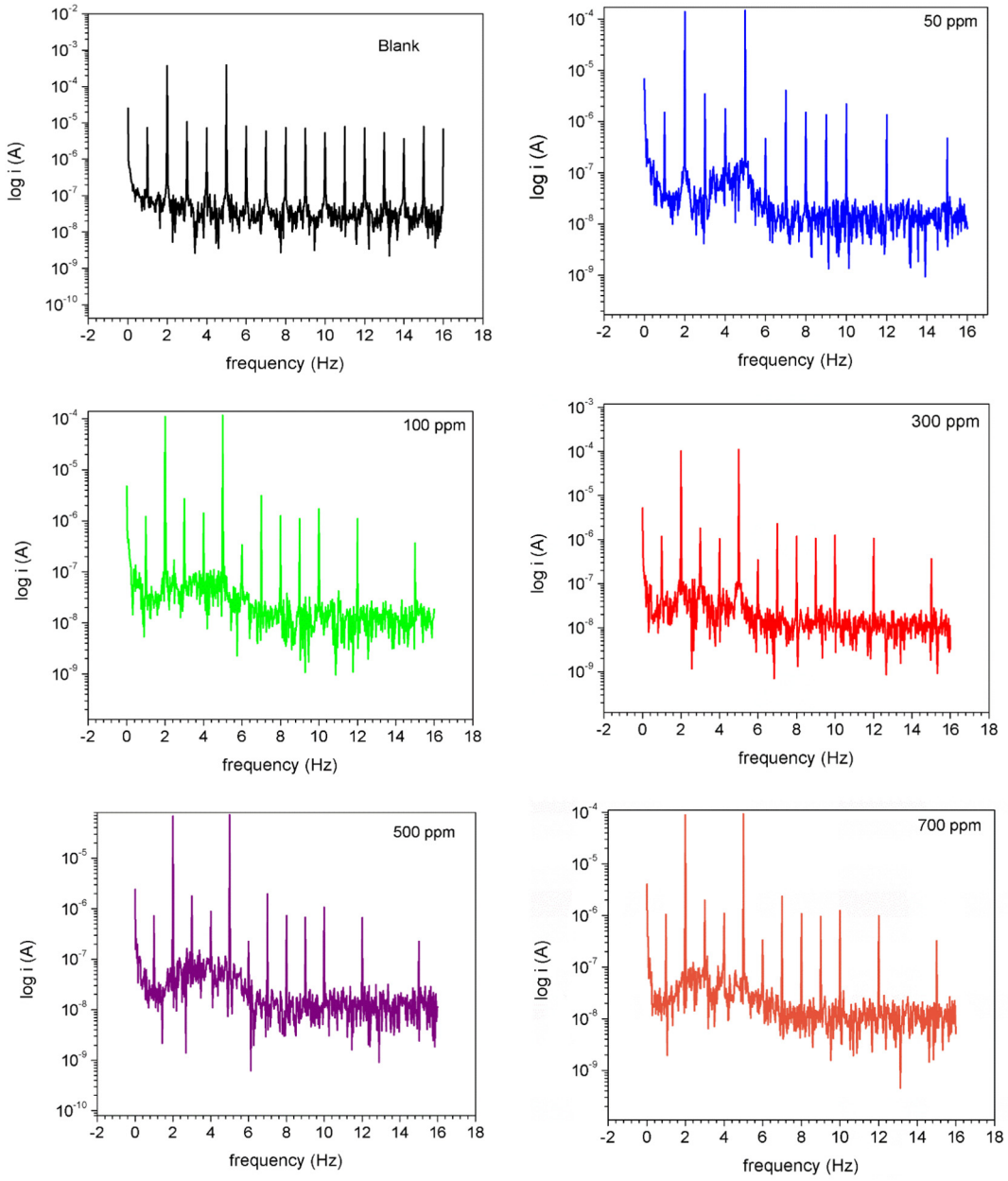

Fig. 5. Intermodulation spectra recorded for St37–2 steel in 15% HCl solution without and with various concentrations of polymer **4** at 25 °C.

Fig. 6 depicts the potentiodynamic polarization (PDP) curves collected for St37–2 steel in 15% HCl solution free from and containing diverse amount of polymer **4** at 25 °C. The values of polarization parameters namely, corrosion potential (E_{corr}), i_{corr}, and the anodic and cathodic slopes (β_a & β_c) derived from the extrapolation of the linear portions of the graphs are displayed in Table 2. It is apparent in Fig. 6 that the presence of polymer **4** in the acid solution greatly decrease both the anodic and cathodic current densities which is a reflection of

Table 2
Electrochemical frequency modulation (EFM), potentiodynamic polarization (PDP), and linear polarization (LPR) parameters for St37–2 steel in 15% HCl solutions in the absence and presence of different concentrations of polymer **4** at 25 °C.

Conc. (ppm)	EFM				PDP					LPR	
	i_{corr} (μA cm^{-2})	CF–2	CF–3	η_{EFM} (%)	$-E_{corr}$ (mV vs. Ag/AgCl)	i_{corr} (μA cm^{-2})	β_a (mV dec^{-1})	β_c (mV dec^{-1})	η_{PDP} (%)	R_p (Ω cm^2)	η_{LPR} (%)
0	928.00	1.69	3.13	–	470.00	422.00	74.10	84.10	–	39.09	–
50	261.00	1.89	3.06	71.88	477.00	167.00	117.40	104.70	60.43	126.10	69.00
100	200.10	1.86	3.30	78.44	468.00	117.00	91.30	97.40	72.27	157.20	75.13
300	182.70	1.78	3.13	80.31	475.00	84.10	74.70	71.10	80.07	167.00	76.59
500	125.50	1.92	3.08	86.48	480.00	42.50	54.50	59.70	89.93	250.20	84.38
700	153.20	1.83	3.10	83.49	469.00	107.00	104.8	129.10	74.64	191.40	79.58

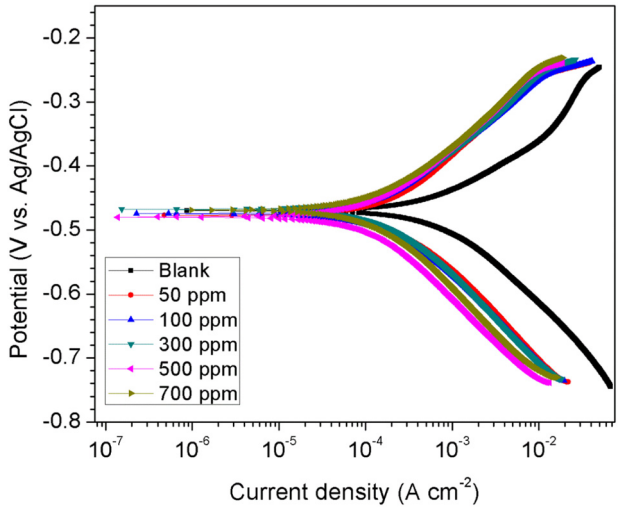

Fig. 6. Potentiodynamic polarization plots for St37–2 steel in 15% HCl solution without and with different concentrations of polymer **4** at 25 °C.

the anticorrosive property of the compound. As clearly seen in the figure, the displacement of the corrosion potential in inhibited systems relative to that of the uninhibited is very minimal. In fact, the difference between the E_{corr} value of the blank and those of the inhibited is in the range of ± 2–10 mV vs. Ag/AgCl. This clearly shows that polymer **4** acted as a mixed type corrosion inhibitor retarding both the anodic iron oxidation and cathodic hydrogen reduction reactions [49,50]. This claim is further supported by the slight changes in both the anodic and cathodic slopes upon addition of inhibitor (Table 2). For instance, the anodic slope of 74.10 mV dec $^{-1}$ and cathodic slope of 84.10 mV dec $^{-1}$ are changed to 54.50 mV dec $^{-1}$ and 59.70 mV dec $^{-1}$ respectively upon addition of 500 ppm polymer **4**. The minimal alteration of the anodic and cathodic slopes by the inhibitor also suggest that the iron dissolution and hydrogen reduction reaction mechanisms was not changed by the inhibitor [51,52]. Corrosion inhibition was therefore achieved by the blocking of active reaction sites. The inhibition efficiency of the optimum concentration from this technique is 89.93%.

The anticorrosion property of polymer **4** was also examined by linear polarization resistance (LPR) technique and the obtained results are listed in Table 2. Clearly, the steel electrode exhibited higher resistance to polarization in acid solution containing polymer **4** than in its absence. As earlier explained, the adsorption of the inhibitor molecules on the electrode surface barricaded the surface from the ingression of aggressive ions present in the environment. The presence of the optimum concentration of the inhibitor in the acidic environment boosted the polarization resistance of the electrode by almost 6%, that is, from 39.09 Ω cm^2 to 250.20 Ω cm^2. It should be mentioned that the inhibition efficiency values obtained from all the electrochemical techniques are in perfect agreement.

3.4. Weight loss studies

The performance of polymer **4** for St37–2 steel in 15% HCl solution in 25 °C was also studied by weight loss approach and the results obtained are presented in Table 3. The results reveal that weight loss and the corrosion rate vary inversely while surface coverage and inhibition efficiency vary directly with increasing inhibitor dosage up to the optimum concentration. The corrosion rate of 87.716 mm/yr declined to 22.290 mm/yr in corrosive system containing 500 ppm polymer **4** and the corresponding η is 74.530%. Although polymer **4** could afford inhibition efficiency of up to 74%, the performance of this polymer is far below the industrial standard. Industrially, corrosion rate of metal in an inhibited corrosive medium is required to be 4 m/y (0.1 mm/y) [53]. The results from weight loss experiments is in conformity with those from the electrochemical techniques (Tables 1 & 2).

Table 3
Calculated values of weight loss (g), corrosion rate (mm per year), surface coverage (θ), and inhibition efficiency (η) for St37–2 steel in 15% HCl solution various concentrations of polymer **4** at 25 °C from weight loss measurements.

Concentration (ppm)	Weight loss (g)	ν (mm p y)	θ	η_{WL}(%)
0	0.213 ± 0.18	43.905	–	–
50	0.075 ± 0.02	15.460	0.648	64.789
100	0.071 ± 0.02	14.635	0.667	66.667
300	0.061 ± 0.04	12.574	0.714	71.362
500	0.045 ± 0.05	9.276	0.789	78.873
700	0.054 ± 0.05	11.131	0.746	74.648

3.5. Effect of KI addition on the performance of polymer 4 as inhibitor

Since the performance of polymer **4** as inhibitor for steel in the simulated acidizing medium even at optimum concentration was unsatisfactory, we added small amount of KI to the polymer as a way of enhancing its effectiveness. Potassium iodide was opted for because of its higher tendency for chemisorption compared to other halide ions [54–56]. The results obtained from weight loss experiments undertaken to examine the performance of polymer **4** + KI mixture on the corrosion of the steel specimen in aggressive 15% HCl medium are given in Table 4. It is very certain from the results in the table that addition of KI to polymer **4** benefitted the inhibition efficiency of the polymer immensely. There is remarkable reduction in the weight loss and corrosion rate of the metal sample in the systems containing the polymer-iodide ions mixture than in system containing the polymer alone (Table 3). In fact, the corrosion rate was reduced from a two-digit value to a single value in all cases. In specific terms, the corrosion rate was decreased from 87.716 mm/yr which is the rate in the unprotected acid solution to 7.636, 4.953, 3.509, 3.096, and 2.683 mm/yr in acid solution inhibited with 50 ppm polymer **4** + 1 mM KI, 100 ppm polymer **4** + 1 mM KI, 300 ppm polymer **4** + 1 mM KI, 500 ppm polymer **4** + 1 mM KI, and 700 ppm polymer **4** + 1 mM KI respectively. The calculated values of surface coverage and inhibition efficiency reveal that over 90% of the metal surface was covered/protected by the adsorbed polymer-iodide ions films in all cases. This noticeable improvement in the performance of polymer **4** could be as a result of synergistic influence which could be ascertained by the calculation of the synergism parameter (S_θ). Generally, S_θ value greater than unity is reflective of synergistic effect, i.e. cooperative co-adsorption while S_θ value less than unity is indicative of antagonistic effect i.e. competitive co-adsorption [35,56,57]. S_θ was calculated using the following equation [57]:

$$S_\theta = \frac{1-(\theta_1+\theta_2-\theta_1\theta_2)}{1-\theta^1_{1+2}} \quad (10)$$

where θ_1 is degree of surface coverage of polymer **4**, θ_2 is the degree of surface coverage of iodide ions and $\theta_{1+2}{}^1$ is the degree of surface coverage of polymer **4** + KI mixture. The calculated S_θ values are

Table 4
Calculated values of weight loss (g), corrosion rate (mm/yr), surface coverage (θ), inhibition efficiency (η), and synergism parameter (S_θ) for St37–2 steel in 15% HCl solution containing various additives at 25 °C from weight loss measurements.

System	Weight loss (g)	ν (mm/yr)	θ	η_{WL}(%)	S_θ
1 mM KI	0.177 ± 0.02	36.485	0.167	16.745	–
50 ppm Polymer 4 + KI	0.037 ± 0.02	7.544	0.828	82.785	1.705
100 ppm Polymer 4 + KI	0.024 ± 0.02	4.968	0.887	88.664	2.455
300 ppm Polymer 4 + KI	0.017 ± 0.03	3.566	0.919	91.863	2.941
500 ppm Polymer 4 + KI	0.015 ± 0.03	3.071	0.930	92.992	2.511
700 ppm Polymer 4 + KI	0.053 ± 0.02	3.154	0.928	92.803	2.939

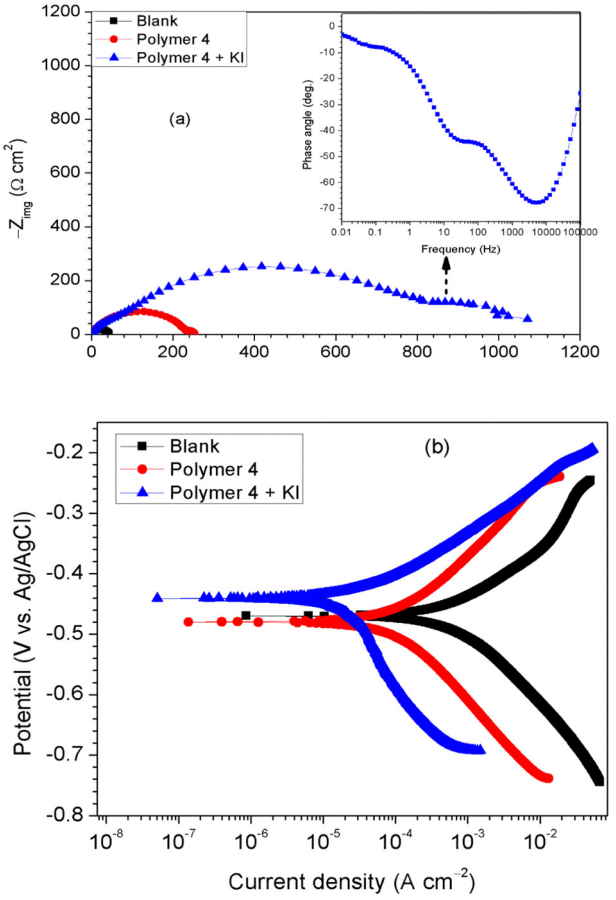

Fig. 7. Comparative (a) electrochemical impedance and (b) potentiodynamic polarization graphs of St37–2 steel in 15% HCl solution without and with the optimum polymer **4** concentration alone and in combination with 1 mM KI at 25 °C.

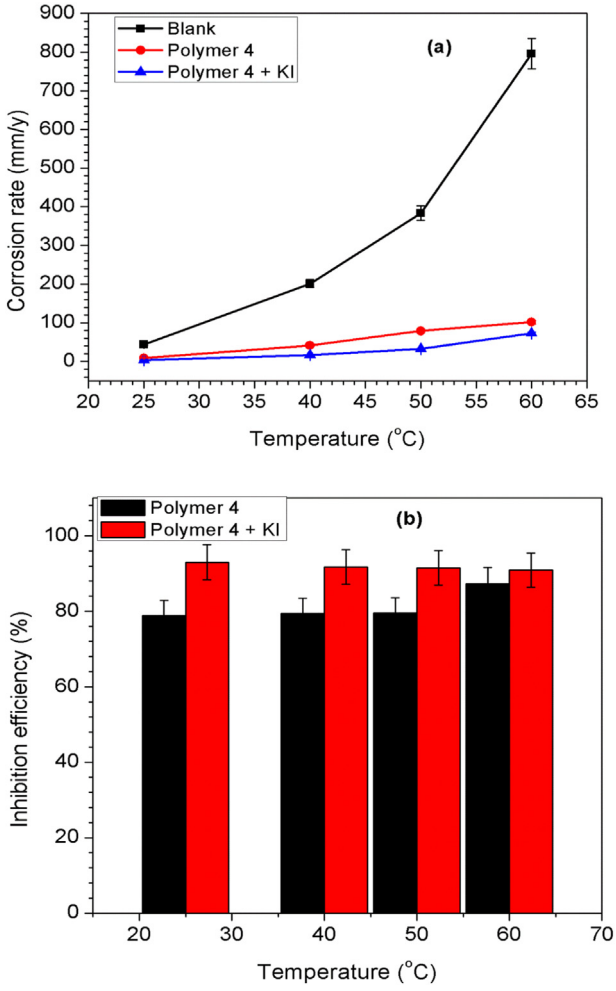

Fig. 8. Variation of (a) corrosion rate of St37–2 steel and (b) inhibition efficiency of polymer **4** and polymer **4** + KI with system temperature.

presented in Table 4. In all cases, S_θ value is greater than unity meaning polymer **4** and iodide ions cooperatively co-adsorbed on the steel surface and protected the surface against corrosion.

The enhanced corrosion inhibition by polymer **4** + KI combination noted from weight loss technique was also verified via EIS and PDP approaches. In these approaches, studies were done utilizing 500 ppm polymer **4** + 1 mM KI mixture only at 25 °C. The results are presented in Fig. 7. In the Nyquist diagram present in Fig. 7(a), the size of the capacitive loop at the high frequency regions in the polymer **4** + KI graph is almost three times that of the polymer **4** graph. This is a clear reflection of the improvement in the resistance of the steel specimen to corrosion in polymer **4** + KI system than in polymer **4** environment. Again, a second capacitive loop occasioned by the double layer structure of the adsorbed polymer **4** + KI film [58–60] is observed in the middle frequency regions. The two semicircles noted in the Nyquist diagram drawn for the polymer **4** + KI system correspond to two times constant which is obvious in the inserted Phase angle plot. Accordingly, a two-time constant equivalent circuit shown in Fig. 4(b) was used for the analysis of the impedance. The physical meanings of the elements in the equivalent circuit are as follow: CPE_{dl} = constant phase element of the inner film, CPE_f = constant phase element of the outer film, R_f = resistance of the outer layer of the adsorbed film, R_s and R_{ct} retain the meanings earlier given in Sub-section 3.2. From the analysis, the R_f and R_{ct} values were obtained to be 47.92 ± 4.60 Ω cm^2 and 858.60 ± 4.41 Ω cm^2 respectively. This reveals a significant boosting of the corrosion resistance property of the metal in the polymer **4** + KI environment in comparison to polymer **4** environment. The charge transfer resistance of the metal substrate is increased by almost 72% in the polymer-iodide ions mixture environment (i.e from 236.80 ± 1.26 Ω cm^2 to 858.60 ± 4.41 Ω cm^2) and the protective efficacy of the mixture is 95.05% which is in good agreement with the results from the weight loss technique. In the comparative polarization curves given in Fig. 7(b), it is clear that the polymer **4** + KI mixture caused greater displacement on both the anodic and cathodic branches than do polymer **4** alone relative to the blank. The corrosion current density was further reduced from 42.50 μA cm^{-2} to 22.70 μA cm^{-2} and inhibition efficiency upgraded from 89.93% to 94.62% upon addition of KI to polymer **4**.

3.6. Effect of temperature on inhibitive performance of polymer 4 and polymer 4 + KI

Weight loss experiments were conducted in 15% HCl solution devoid of and containing 500 ppm polymer **4** or 500 ppm polymer **4** + 1 mM KI at 25–60 °C in order to examine the influence of temperature on the corrosion of St37–2 steel and on the corrosion inhibition efficiency of the additives. The results obtained are presented in Fig. 8. As could be seen in Fig. 8(a), increase in the system temperature accelerated the dissolution of the metal specimen particularly in the unprotected acid solution. The corrosion rate at 60 °C is almost 18 times the value at 25 °C, i.e. 43.905 mm/yr at 25 °C and 796.270 mm/yr at 60 °C. In the inhibited acid solution, the corrosion rate is remarkably reduced even at elevated temperatures. In fact, the corrosion rate is decreased by 87.26% and 90.88% in the polymer **4** and polymer **4** + KI systems respectively at 60 °C. In Fig. 8(b), the inhibition efficiency (η) of

polymer **4** increases with rise in temperature. The η value increased from 78.87% at 25 °C to 87.26% at 60 °C. This trend is common with chemisorption mechanism [10]. Polymer **4** molecules could interact chemically with the steel surface using the electron pair on its nitrogen atom (see polymer **4** structure in Scheme 1) and the vacant d-orbital of Fe. In the case of polymer **4** + KI, η slightly decreased with increasing temperature. For instance, the value declined from 92.96% at 25 °C to 90.89% at 60 °C. This suggests physisorption mechanism [14] and the decline in η may infers desorption of some adsorbed additive film at elevated temperature. A close inspection of Fig. 8(b) reveals that the η was near constant at 40 and 50 °C. The η is 91.70% (~92%) at 40 °C and 91.50% (~92%) at 50 °C. The reason for the near constancy is unclear. However, several explanations have been advanced by corrosion scientists. One of such and the most convincing is the formation of dimeric layer on a metal surface [14,61]. In such a situation, increase in temperature will cause the desorption of the outer layer of the adsorbed film why the underlying layer continue to offer protection against corrosion. It has also been opined that inhibitor structural transformation and rearrangement on a substrate surface at elevated temperatures could also give rise to near constancy of inhibition efficiency [14].

As noted above, temperature had noticeable influence on the corrosion rate of the studied metal specimen in the corrosive environment. The Arrhenius equation (Eq. (11)) is suited for describing the dependency of corrosion rate on temperature.

$$\log \nu = \log A - \frac{E_a}{2.303RT} \tag{11}$$

where ν is the corrosion rate, R the molar gas constant, E_a is the activation energy, and T the absolute temperature. The plots of log ν as a function of $1/T$ drawn for the studied systems are given in Fig. S2(a) in the supporting information. From the slope (E_a/2.303RT) of the graphs, the E_a was calculated to be 69.239 kJ mol^{-1}, 61.890 kJ mol^{-1}, and 76.962 kJ mol^{-1} for the blank, polymer **4**, and polymer **4** + KI inhibited systems respectively. The value of E_a has been used by many authors to pinpoint on the predominant adsorption mechanism of organic inhibitors [57,60,62,63]. When E_a in an unprotected corrosive environment is less than the E_a of a protected environment, the inhibitor is believed to exhibits electrostatic character, i.e. physisorption [63]. In the other hand, when the E_a in a protected corrosive system is less than the E_a of unprotected, chemisorption mechanism is believed to play the dominant role [10]. On this backdrop, the prevailing mechanism in the acid solution containing polymer **4** is chemisorption while physisorption is the dominant mechanism in the polymer **4** + KI system. As indicated by the synergism parameter value (Table 4), iodide ions first adsorbed chemically on the steel surface, replenished the surface before cationic form of polymer **4** electrostatically adsorbed on the iodide ions layer.

The alternative form of Arrhenius equation is called the Transition State equation and can be written as:

$$\log \frac{\nu}{T} = \left[\left(\log\left(\frac{R}{Nh}\right) + \left(\frac{\Delta S_a}{2.303R}\right)\right)\right] - \frac{\Delta H_a}{2.303RT} \tag{12}$$

where N is the Avogadro's number, h is the Planck's constant, ΔH_a is the enthalpy of activation, and ΔS_a the entropy of activation. A plot of log ν/T against $1/T$ resulted in a linear graph given in Fig. S2(b). From the slope and intercept of the graphs, the values of ΔH_a and ΔS_a were computed. The calculated ΔH_a value is 57.066 kJ mol^{-1}, 45.601 kJ mol^{-1}, and 67.938 kJ mol^{-1} while the ΔS_a value is −19.404 J/mol K, − 69.618 J/mol K, and – 6.138 J/mol K for the blank, polymer **4**, and polymer **4** + KI systems respectively. The ΔH_a values are positive implying endothermic corrosion process [14] and are less than the E_a values which is in conformity with the famous thermodynamic equation, $E_a - \Delta H_a = RT$. The ΔS_a value calculated for polymer **4** protected acid medium is more negative than that of the blank suggesting less perturbed system during the formation of Fe– polymer **4** complex than during Fe–H_2O formation [62]. It is however observed that the ΔS_a value for polymer **4** + KI system is nobler than that of the blank. Similar observation had been reported by Biswas et al. [8]. It implies a more random arrangement of the polymer **4** + KI system. It should be recalled that corrosion inhibition by organic inhibitor is a quasi-substitution process whereby adsorbed water molecules are replaced by

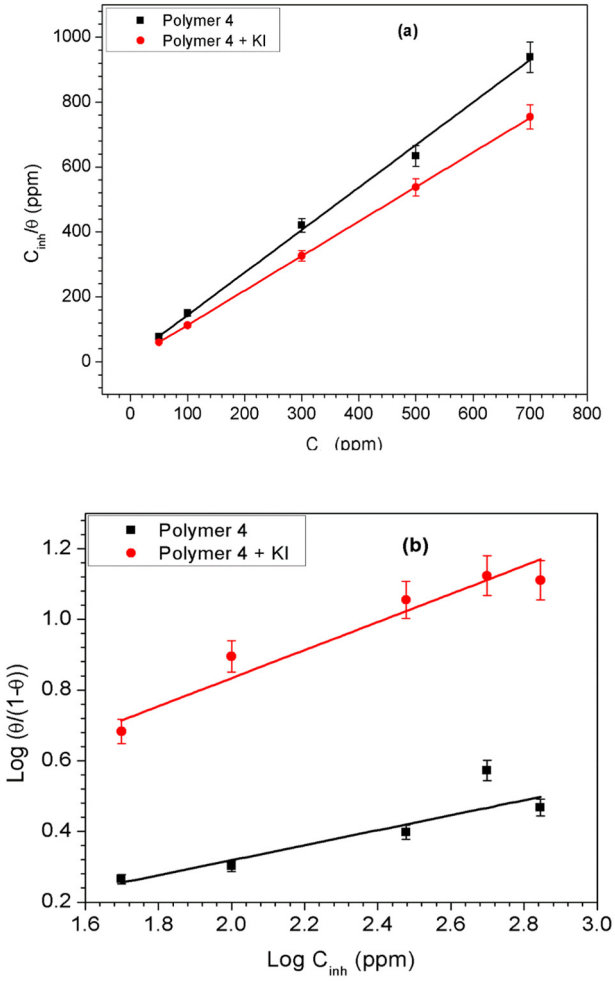

Fig. 9. (a) Langmuir and (b) El-Awady et al. adsorption isotherm plots for the adsorption of polymer **4** alone and in combination with KI onto St37–2 steel surface in 15% HCl solution at 25 °C.

Table 5
Adsorption parameters for St37–2 steel in 15% HCl solution containing polymer **4** and polymer **4** + KI mixture at 25 °C.

System	Langmuir				El-Awady et al.			
	slope	K_{ads} (ppm mol^{-1})	$-\Delta G_{ads}^0$ (kJ mol^{-1})	R^2	1/y	K_{ads} (ppm mol^{-1})	$-\Delta G_{ads}^0$ (kJ mol^{-1})	R^2
Polymer 4	1.310	75.766	44.951	0.997	4.721	78.560	45.041	0.827
Polymer 4 + KI	1.063	141.806	46.504	0.999	2.516	109.219	45.857	0.928

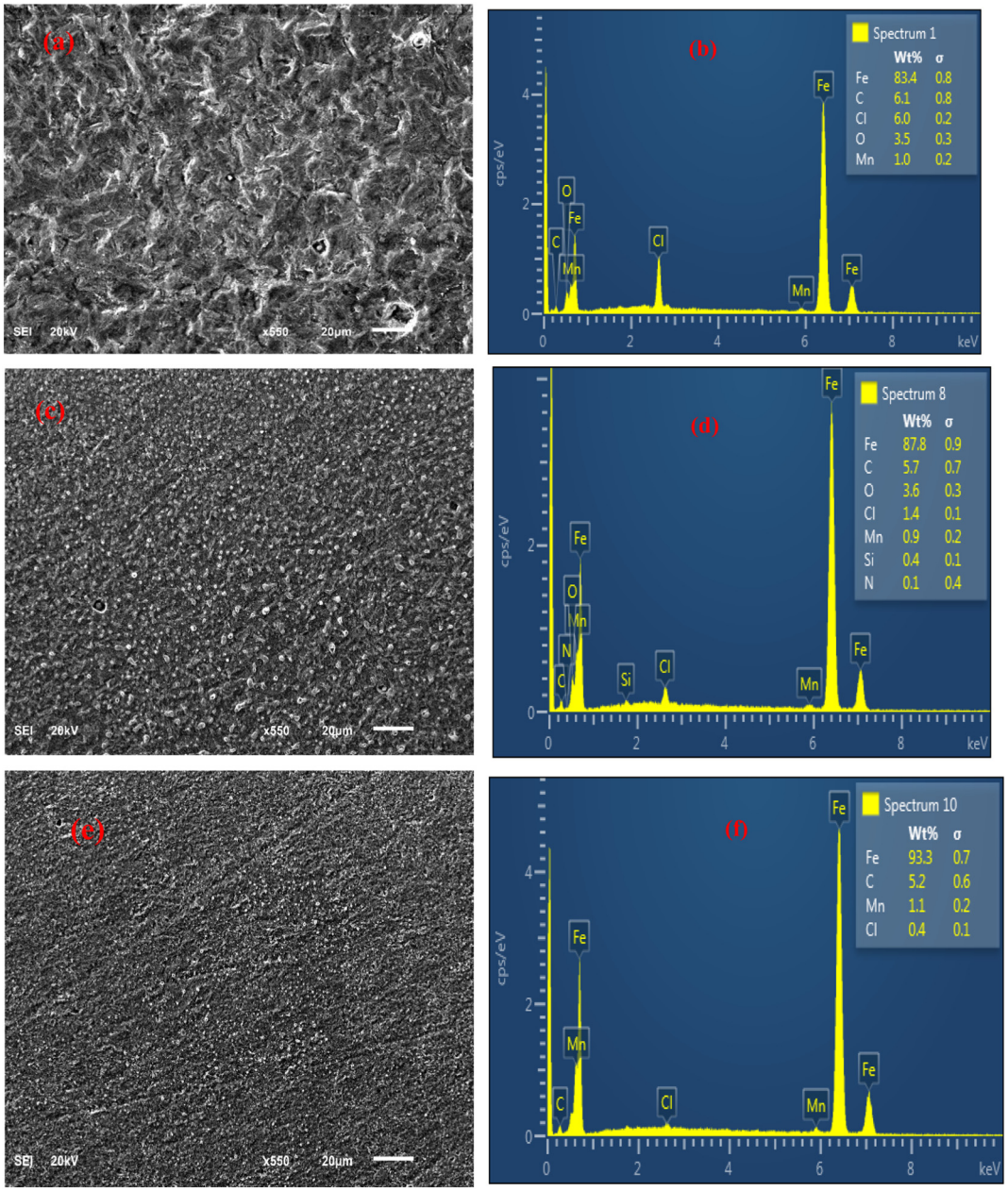

Fig. 10. SEM pictures and EDAX spectra for St37–2 steel specimen after immersion in 15% HCl solution (a, b) without inhibitor, (c, d) containing 500 ppm polymer **4**, and (e, f) containing 500 ppm polymer **4** + 1 mM KI for 24 h at 25 °C.

organic inhibitor molecules [10,14,61]. Therefore, the entropy of activation is the summation of the entropies associated with the desorption of water molecules and adsorption of organic inhibitor molecules [8]. The observed gain in entropy in the polymer **4** + KI inhibited system may be due to an increase in the solvent entropy [8,50].

3.7. Adsorption consideration

In order to explain the adsorption and the strength of interaction between polymer **4** or polymer **4** + KI with St37–2 steel surface, the surface coverage values given in Tables 3 or 4 were fitted into various adsorption isotherms. The linear regression coefficient (R^2) value was used as a gauge in selecting the isotherm that best fit the experimental data. It was found to be the Langmuir adsorption isotherm as R^2 value of approximately one was obtained (Table 5). The Langmuir adsorption model assumes that (i) adsorbate molecules adsorb only on fixed adsorption sites on solid adsorbent surface, (ii) all active sites on substrate surface have equivalent energy, (iii) the substrate surface is completely flat and uniform on microscopic dimension, (iv) monolayer of adsorbate is formed on adsorbent surface, and (v) adsorbed molecules on substrate surface are free of interaction with each other. The Langmuir adsorption isotherm has the form:

$$\frac{C_{inh}}{\theta} = \frac{1}{K_{ads}} + C_{inh} \tag{13}$$

where C_{inh} is the concentration of inhibitor, K_{ads} is adsorption-desorption equilibrium constant and define the stamina of the bond between adsorbent and adsorbate [10]. A plot of C_{inh}/θ versus C_{inh} for the investigated systems is shown in Fig. 9(a). From the slope of the graphs, K_{ads} value was calculated and listed in Table 5. The large K_{ads} value is indicative of strong interaction between the additives and the metal surface. However, polymer **4** + KI mixture formed a stronger bond with the steel surface than polymer **4** at 25 °C and was translated into a better inhibition performance (Table 4). If the assumption of a non-

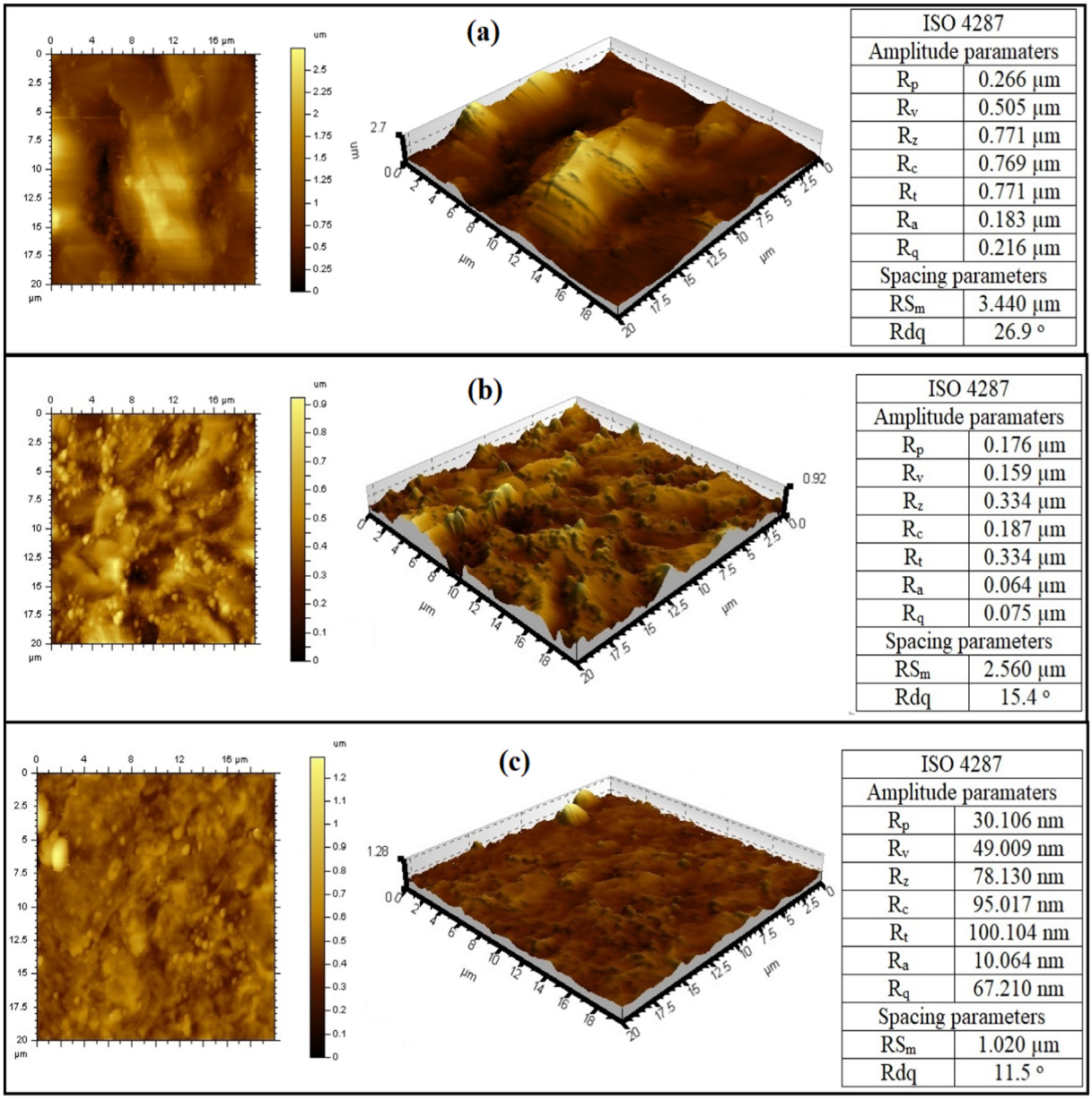

Fig. 11. AFM images in 2D and 3D formats for St37–2 steel specimen after immersion in 15% HCl solution (a) without inhibitor, (b) containing 500 ppm polymer **4**, and (c) containing 500 ppm polymer **4** + 1 mM KI for 24 h at 25 °C. Inserted table shows the roughness parameters as defined by the ISO 4287 standard.

interplay between adsorbed molecules is valid, the slope of Langmuir plot would be unity. The slope obtained in our case (Table 5) slightly deviated from unity meaning that there was interaction of adsorbed species on the substrate surface. The alternative form of Langmuir adsorption isotherm called El-Awady et al. kinetic-thermodynamic model takes into consideration interaction of adsorbed species [43]. This model was therefore adopted to verify if actually there was interplay of adsorbed molecules on the metal surface. The El-Awady et al. kinetic-thermodynamic isotherm assumes the form:

$$\log\left(\frac{\theta}{1-\theta}\right) = \log K_{ads} + y \log C_{inh} \tag{14}$$

where 1/y denotes the number of active sites occupied by inhibitor or the number of water molecules displaced by an inhibitor molecule [60]. Fig. 9(b) shows the El-Awady et al. kinetic-thermodynamic isotherm plots for the adsorption of polymer **4** alone and in combination with KI onto St37–2 steel surface in 15% HCl solution at 25 °C. The R^2 value is 0.827 and 0.928 for the two investigated systems meaning the model can be used to describe the adsorption process. The K_{ads} values obtained from this model are in perfect agreement with those from the Langmuir adsorption plot (Table 5). It is obvious that polymer **4** and polymer **4** + KI adsorbed molecules occupied more than one active site on the metal surface; 1/y is greater than unity.

The adsorption-desorption equilibrium constant is related to the standard adsorption free energy (ΔG_{ads}^{0}) according to the following equation [64]:

$$\Delta G_{ads}^{0} = -RT \ln(1 \times 10^{6} K_{ads}) \tag{15}$$

where 1×10^6 is the dosage of water molecules in mg/L or ppm (same as dosage of inhibitor), R and T are the molar gas constant (8.3144598 J/K) and absolute temperature respectively. The calculated ΔG_{ads}^{0} value from the two isotherm models is also presented in Table 5. The low values of ΔG_{ads}^{0} (up to -45 kJ mol^{-1}) and the high K_{ads} values are reflective of firm adherence of adsorbed additive molecules. In fact, most authors associate ΔG_{ads}^{0} value of up to -40 kJ mol^{-1} to chemisorption mechanism. Han et al. [36] reported ΔG_{ads}^{0} of

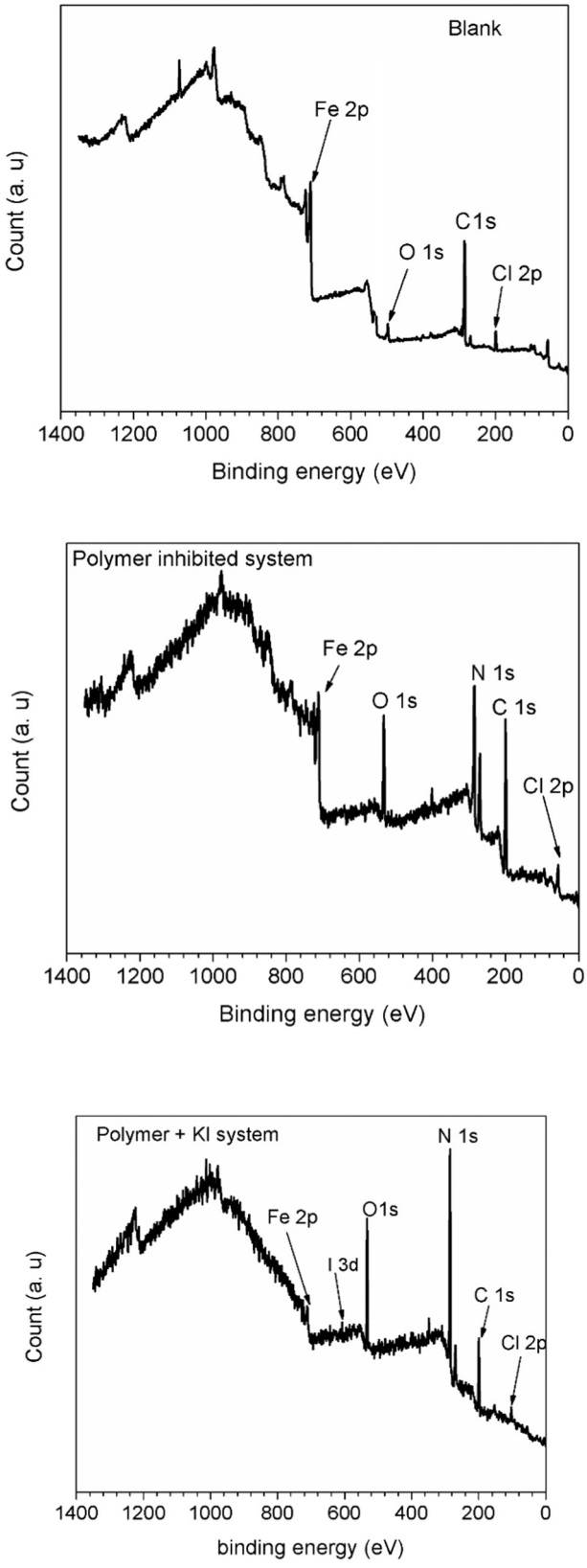

Fig. 12. XPS survey spectra of St37–2 steel specimen surface immersed in 15% HCl solution without and with additives for 24 h at 25 °C.

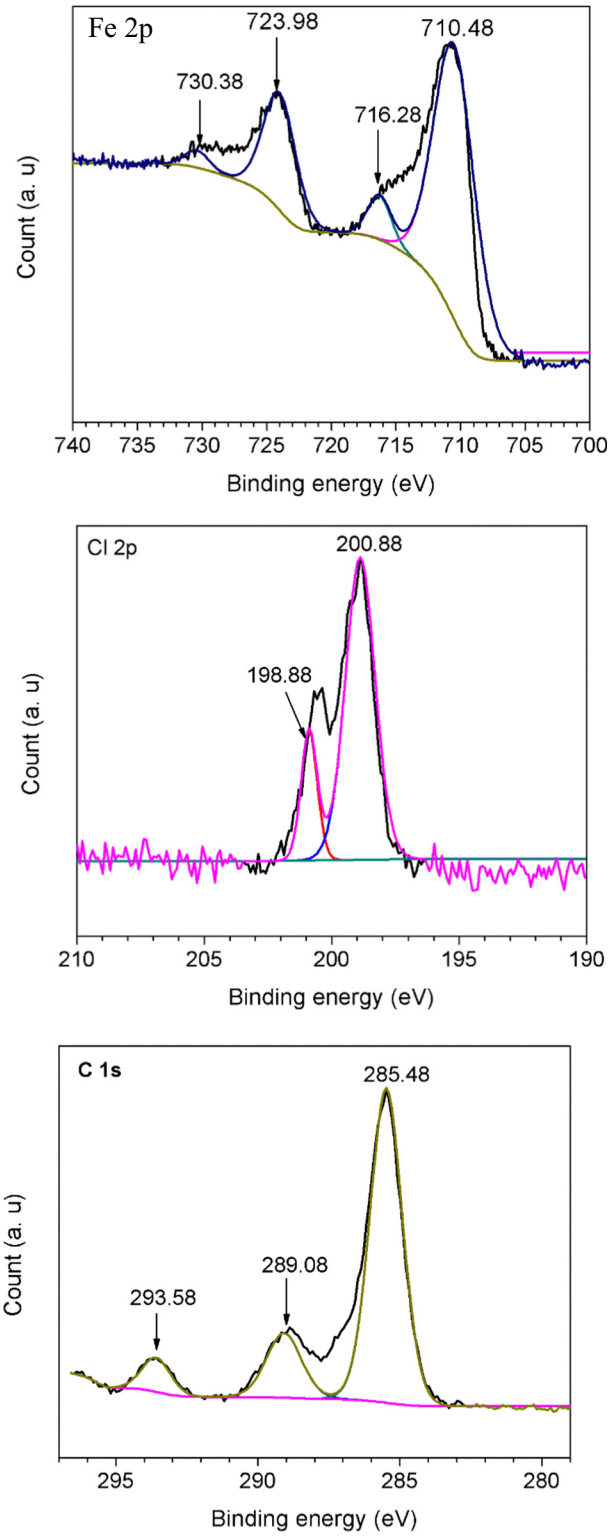

Fig. 13. High resolution XPS spectra of the corrosion products formed on St37–2 steel specimen surface immersed in 15% HCl solution for 24 h at 25 °C.

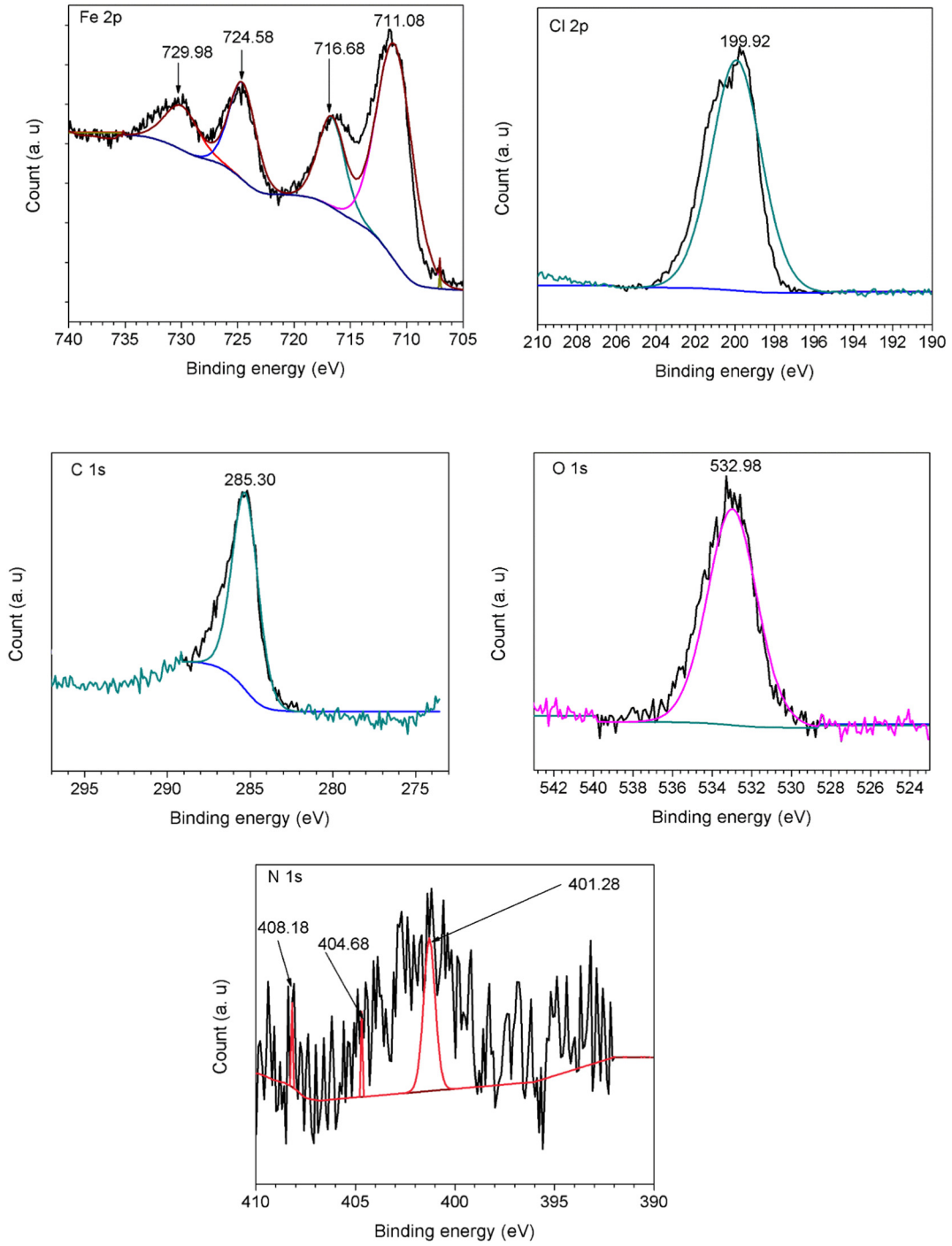

Fig. 14. High resolution XPS spectra of the adsorbed film on St37–2 steel specimen surface immersed in 15% HCl solution containing 500 ppm polymer **4** for 24 h at 25 °C.

$-54.27\ kJ\ mol^{-1}$ and $-55.72\ kJ\ mol^{-1}$ for the chemical adsorption of imidazoline quaternary salt/benzotriazole and imidazoline quaternary salt/octyl phenol ethoxylate mixtures respectively on steel surface in 10% HCl solution. For the chemical adsorption of polypropylene glycol/silver nanoparticle composites on mild steel surface in sulfuric acid medium at 333 K, value reported was $-40.72\ kJ\ mol^{-1}$ [65].

3.8. Surface examination

3.8.1. SEM and EDAX studies

Fig. 10 shows the SEM pictures and EDAX spectra obtained for St37–2 steel sample after exposing to 15% HCl solution (a, b) free of inhibitor, and containing (b, c) 500 ppm polymer **4**, (e, f) 500 ppm polymer **4** + 1 mM KI mixture for 24 h at 25 °C. In the free acid solution, the sample suffered severe surface damage due to corrosive attack and the surface looks rough (Fig. 10(a)). Some cracks can even be spotted in the surface in Fig. 10(a). This surface, according to the EDAX spectrum in Fig. 10(b) was rich in chloride ions (6.0%) which is in accordance with the general mechanism summarized in Eqs. (16)–(19) [66,67].

$$Fe + Cl^{-} \leftrightarrow (FeCl^{-})_{ads} \quad (16)$$

$$(FeCl^{-})_{ads} \leftrightarrow (FeCl)_{ads} + e^{-} \quad (17)$$

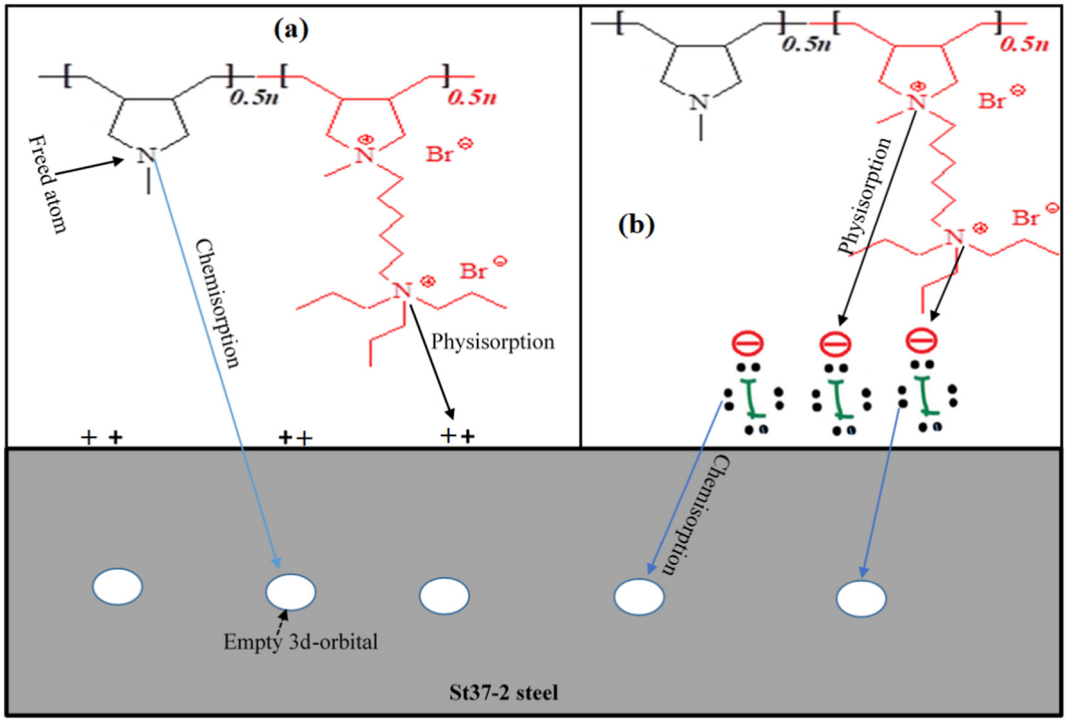

Fig. 15. Illustration of the mechanism of corrosion inhibition by (a) polymer **4** and (b) polymer **4** + KI mixture.

$$(FeCl)_{ads} \rightarrow (FeCl^{+}) + e^{-} \quad (18)$$

$$(FeCl^{+}) \leftrightarrow Fe^{2+} + Cl^{-} \quad (19)$$

In the acid solution fortified with the additives, the steel specimen suffered less corrosive attack as evident in the smoother surfaces in Fig. 10(c & e) relative to the surface in Fig. 10(a). It is observed from Fig. 10(d & f) that chloride ions content was less in the surfaces of the specimens immersed in 15% HCl solution containing polymer **4** or polymer **4** + KI mixture. The chloride ions content in these surfaces is 1.4% and 0.4% respectively. It could be that the polymer intercepted the Fe oxidation reaction by adsorbing onto the metal surface according to the following equation:

$$(FeCl^{-})_{ads} + \text{polymer } \mathbf{4}^{+} \rightarrow (FeCl^{-}\text{polymer } \mathbf{4}^{+})_{ads} \quad (20)$$

The appearance of nitrogen band which is a component element of the studied inhibitor in the spectrum in Fig. 10(d) and its absence in the spectrum in Fig. 10(a) provides an experimental evidence to the claim of inhibitor adsorption on the metal surface. Meanwhile, the better corrosion inhibition performance by polymer **4** + KI mixture than polymer **4** alone noted from the experimental results (Tables 3 & 4) is also obvious in the SEM pictures. The surface in Fig. 10(e) is smoother than the one in Fig. 10(c).

3.8.2. AFM studies

AFM experiments were performed to determine the surface roughness of St37–2 steel specimen exposed to 15% HCl solution without and with inhibitor for 24 h at 25 °C. The 2D and 3D images obtained are shown in Fig. 11. The measured values for the basic surface roughness parameters contained in the International Organization of Standardization (ISO) 4287 are displayed in the inserted tables. The description of the parameters is as follow; R_p = maximum band height, R_v = maximum valley depth, R_z = mean band to valley height, R_c = mean band to valley height with no limit to the amount of bands and valleys, R_t = largest band to valley height; R_a = mean value of profile deviation from mean line, R_q = root-mean-square deviation from a profile, RS_m = mean spacing of profile elements, and Rdq = root mean square slope of examined profile [60,68,69]. A very rough surface is seen in Fig. 11(a) with Rdq measuring 26.9°. Apparently, the polymer protected the substrate surface against corrosive attack. As could be seen in Fig. 11(b), the surface is smoother compared to the one in Fig. 11(a) and all the roughness parameters have lesser values. The Rdq is decreased by almost 43%, i.e. from 26.9° to 15.4°. The best protection to the metal surface was in acid solution fortified with polymer **4** + KI mixture. By comparing the 2D and 3D images in Fig. 11(a) and (b) to Fig. 11(c), it could be seen that the surface in Fig. 11(c) is the smoothest. Interestingly, the roughness parameters in the table inserted in Fig. 11(c) are all in nm and not in μm as those inserted in Fig. 11(a & b). This is a clear demonstration of the excellent protection offered by the polymer-iodide ions blend to the steel surface.

3.8.3. XPS studies

The surface of St37–2 steel specimen immersed in 15% HCl solution without and with inhibitor for 24 h at ordinary temperature was screened using X-ray Photoelectron Spectroscopy (XPS) to ascertain the chemical elemental composition of the surface. The results obtained are presented in Fig. 12. The elements detected on the sample surface exposed to the blank acid solution include, Fe, O, C, and Cl. The oxygen detected on this surface may have been from adsorbed water [70]. In addition to the elements detected on the sample surface exposed to the free acid solution, N was detected on the surface exposed to acid solution containing polymer **4** while N and I were detected on the surface exposed to 15% HCl solution containing polymer **4** + KI. These elements are components of the added inhibitor and therefore provide experimental evidence to the claim that the adsorption of the additives onto the St37–2 steel sample surface was responsible for the corrosion mitigation noted in the acid solutions fortified with the additives.

3.9. Mechanism of corrosion inhibition by polymer 4 and polymer 4 + KI

In order to explain the corrosion inhibition mechanism by polymer **4** and polymer **4** + KI, the products deposited on the surface of St37–2 specimen exposed to 15% HCl solution free from and containing inhibitor were analyzed via XPS technique. The XPS high resolution spectra of Fe 2p, Cl 2p, and C 1 s for the corrosion products formed on

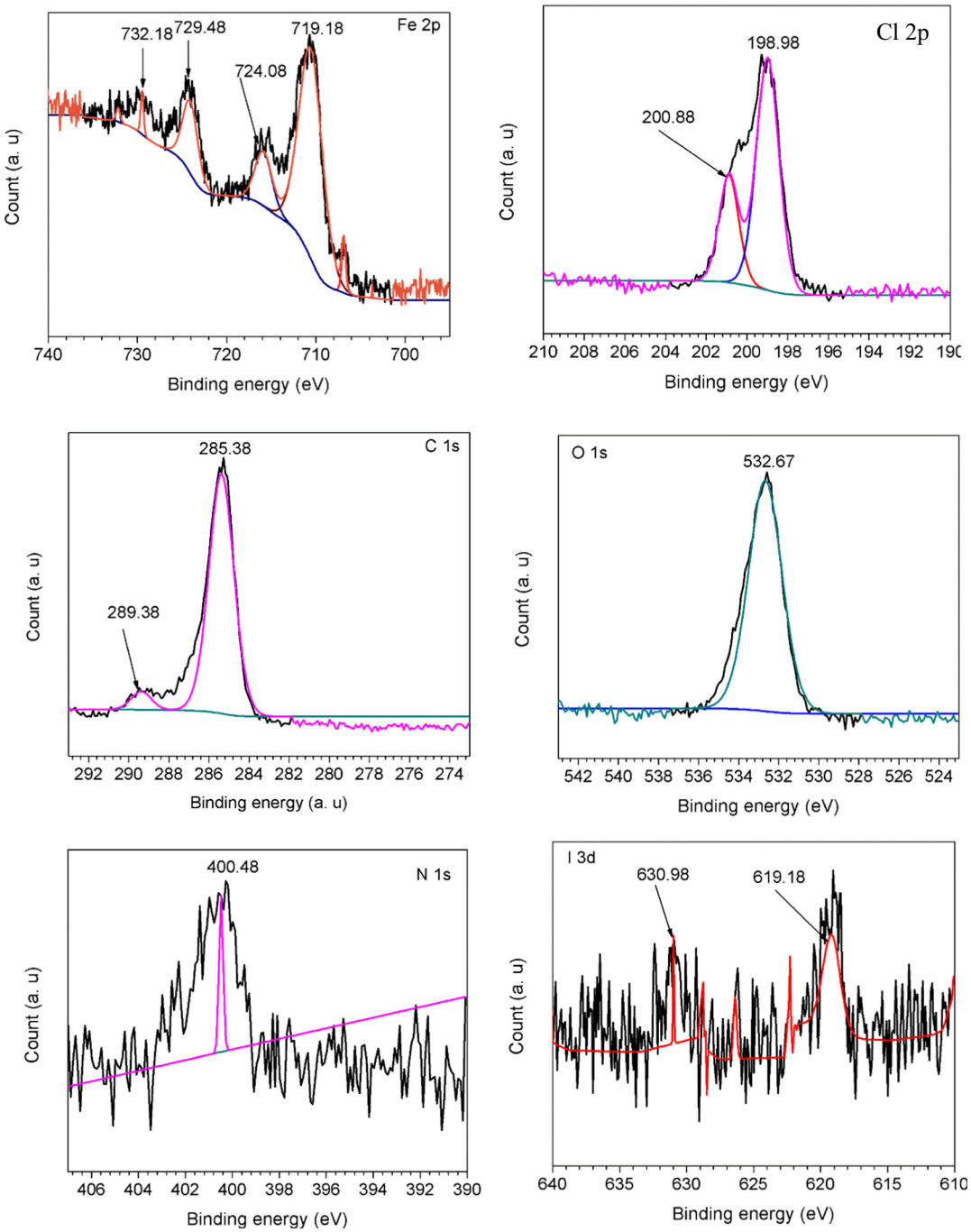

Fig. 16. High resolution XPS spectra of the adsorbed film on St37–2 steel specimen surface immersed in 15% HCl solution containing 500 ppm polymer **4** + 1 mM KI for 24 h at 25 °C.

St37–2 steel specimen surface immersed in blank acid solution is shown in Fig. 13. The Fe 2p structure exhibits a complex nature with series of energy peaks which is occasioned by the presence of doublets of Fe species like Fe^0, Fe^{2+}, Fe^{3+}, as well as the satellites of Fe^{3+} [71]. The notable peaks are at 710.48 eV, 716.28 eV, 723.98 eV, and 730.28 eV and are assigned to Fe^{2+} [72,73], satellites of Fe^{3+} [74,75], Fe^{3+} [75], and ferrhydrates [60,76] respectively. In the Cl 2p spectrum, two energy peaks are identified at 198.88 eV and 200.88 eV and are characteristic signals of Cl $2p_{3/2}$ [75,77] and Cl $2p_{1/2}$ [75,77] respectively. These peaks are associated with the Fe—Cl bond in chlorides like $FeCl_2$ and $FeCl_3$ [75,77] which is in line with the general corrosion mechanism of steel in HCl environment as outlined in Eq. (16)–(19). The C 1 s spectrum in Fig. 13 exhibits three obvious energy bands at 285.48 eV, 289.08 eV, and 293.58 eV. The peaks at 285.48 eV and 289.08 eV are assigned to C—O [74,75] and O–C = O [74,75] signals. The metal seems to have contained or contaminated with elements like K and is responsible for the π-π* satellite signal observed at 293.58 eV. From the analysis, it is obvious that the corrosion products on the specimen surface was a mixture of chlorides, oxides, carbonates, and hydroxides.

Fig. 14 shows the high resolution XPS spectra of the adsorbed film on St37–2 steel specimen surface immersed in 15% HCl solution protected with polymer **4** for 24 h at 25 °C. By comparing the individual spectrum to the one in Fig. 13, some striking difference can be spotted. In the Fe 2p spectrum in Fig. 14, the Fe^{2+}, Fe^{3+}, and ferrhydrates peaks are seen at 711.08 eV, 724.58 eV, and 729.98 eV respectively. The

atomic weight of these components is altered in this surface. In the surface depicted by Fig. 13, the % atomic weight of Fe^{2+}, Fe^{3+}, satellites of Fe^{3+}, and ferrohydrates was 67.96%, 6.30%, 23.20% and 2.54% but 53.60%, 17.00%, 18.48%, and 10.72% respectively on the surface exposed to the inhibited acid solution. The Cl $2p_{3/2}$ peak in the Cl 2p spectrum in Fig. 13 is absent in Fig. 14 while the Cl $2p_{1/2}$ peak shifted to 199.92 eV in Fig. 14. Again, the C 1 s spectrum in Fig. 14 exhibits a single band at 285.30 eV instead of three peaks observed in the C 1 s spectrum in Fig. 13. As earlier mentioned, nitrogen, a component element of the inhibitor is present in the surface exposed to the protected medium. In the N 1 s spectrum in Fig. 14, the energy band at 401.28 eV is assigned to $C–N^+$ [77] and has % atomic weight of 86.97%. All these changes reflect the fact that products deposited on the surface of the steel sample exposed to polymer **4** inhibited system was somewhat different from the products on the metal surface exposed to the uninhibited acid solution. In HCl solution, Fe dissolution proceed according to Eqs. (16)–(19). Our EDAX (Fig. 10(b)) and the XPS results clearly affirm that the surface of St37–2 sample was indeed hydrated with chloride ions. Nitrogen atom is highly basic and is protonated in the studied acid solution as revealed by the XPS result. Predominantly, polymer **4** will exist as polycation, $[\text{polymer } \mathbf{4}]^+$ in the acid solution. Through columbic attraction, the polycations will be attracted to the surface of the metal and the Fe dissolution reaction will be intercepted as illustrated in Eq. (20). On the surface, deprotonation may occur [60,77] such that some of the heteroatoms are freed. Electron pair could be transferred from the freed heteroatoms to the empty 3d-orbital of Fe and by so doing chemical bonds are formed between Fe and the inhibitor molecules [60,78]. This mechanism which is illustrated in Fig. 15(a) is supported by the experimental results given in Fig. 8(b).

Fig. 16 depicts the high resolution XPS spectra of the adsorbed film on the specimen surface immersed in 15% HCl solution containing polymer **4** + I^- ions mixture for a day at 25 °C. In addition to the elements (Fe, Cl, C, O, & N) found on the sample surface exposed to the polymer **4** inhibited acid solution (Fig. 12), I 3d was noted on the surface exposed to the polymer **4** + KI fortified environment. The I 3d spectrum exhibits the I $3d_{3/2}$ and I $3d_{5/2}$ characteristic bands at 619.18 eV and 630.98 eV respectively. Some authors [60,79] had reported similar results and the peak at 619.18 eV was associated with triiodide (I_3^-) while the band at 630.98 eV was for pentaiodide (I_5^-) ions. The value of the synergism parameter given in Table 4 indicates that the adsorption of polymer **4** and iodide ions on steel surface was a cooperative co-adsorption. It means I_3^- and I_5^- ions first adsorbed on the metal surface and because of their higher ionic radius than Cl^- ions appreciably recharged the surface allowing significant amount of $[\text{polymer } \mathbf{4}]^+$ to be adsorbed (Fig. 15(b)). In other words, iodide-$[\text{polymer } \mathbf{4}]^+$ adsorbed layer was thicker than chloride-$[\text{polymer } \mathbf{4}]^+$ layer and as a consequence, the corrosion inhibition strength of the polymer was enhanced (Table 4).

4. Summary and conclusions

There have been concerted effort to synthesize soluble polymeric compounds for corrosion inhibition purposes. We have synthesized poly (DAMA-*ran*-DAMTDB) **4** from inexpensive diallylmethylamine via Butler's cyclopolymerization technique and characterized by ^1H NMR, FTIR, and elemental analysis. The anticorrosion property of the synthesized polymer has been studied for low carbon steel in 15% HCl solution using weight loss, EIS, PDP, EFM, and LPR techniques. The analysis of the metal specimen surfaces exposed to uninhibited and inhibited acid solutions has been performed using SEM, EDAX, AFM, and XPS. Polymer **4** is effective inhibitor with the optimum concentration (500 ppm) affording the highest inhibition efficiency of up to 87% at elevated temperatures. Corrosion mitigation by the polymer is through adsorption, i.e. chemisorption mechanism. Polymer **4** behaved as a typical mixed type corrosion inhibitor retarding both anodic and cathodic corrosion processes. The corrosion mitigation capacity of polymer **4** can be appreciably enhanced by the addition of a minute amount of iodide ions. Protection effectiveness of 93% is achievable with 500 ppm polymer **4** + 1 mM KI mixture at ordinary temperature. The adsorption of polymer **4** and polymer **4** + KI mixture onto St37–2 steel surface in the studied corrosive medium can best be explained using both the Langmuir and El-Awady et al. kinetic-thermodynamic adsorption isotherms. Results from surface examinations are in good agreement with those from experimental and indicate corrosion inhibition by adsorption of the additive molecules on the substrate surface. Corrosion products on steel surface exposed to the free acid solution are mixtures of chlorides, carbonates, oxides, and hydroxides. In polymer **4** + KI system, the polymer molecules are adsorbed on triiodide and pentaiodide ions layer according to XPS results. The enhanced corrosion inhibition of the polymer by iodide ions is synergistic in nature according to the value of calculated synergism parameter.

Declaration of conflict of interest

The authors wish to state that no conflict of interest exist with this manuscript.

Appendix A. Supplementary data

Supplementary data to this article can be found online at https://doi.org/10.1016/j.msec.2019.03.057.

References

[1] IBISWorld, Global oil & gas exploration & production US industry market research report, www.ibisworld.com/industry-trends/global-industry-reports/mining/oil-gas-exploration-production.html, (March 2018).

[2] G. L. McClung IV. Acidizing materials and methods and fluids for earth formation protection. US 20130333892 A1, U.S. Patent 2013, Application No. 13/815,494.

[3] L. Kalfayan, Production Enhancement with Acid Stimulation, Pennwell Books, Tusla, Okla, 2008.

[4] J. P. Engle, B. R. Keeney. Prevention of ferric ion corrosion using acid cleaning solution containing hydrogen sulfide and an aldehyde corrosion inhibitor. US Patent No. 3514410, May 26, 1970.

[5] B. R. Keeney. Corrosion inhibitor composition. US Patent No. 3404094, October 1, 1964.

[6] H. T. Harrison, B. D. Oakes. Corrosion inhibitor composition. US Patent No. 3107221, October 15, 1963.

[7] R. F. Monroe, F. J. Lowes, G. L. Foster, B. D. Oakes. US Patent No. 2993863, July 25, 1961.

[8] A. Biswas, S. Pal, G. Udayabhanu, Experimental and theoretical studies of xanthan gum and its graft co-polymer as corrosion inhibitor for mild steel in 15% HCl, Appl. Surf. Sci. 353 (2015) 173–183.

[9] A. Zeino, I. Abdulazeez, M. Khaled, M.W. Jawich, I.B. Obot, Mechanistic study of polyaspartic acid (PASP) as eco-friendly corrosion inhibitor on mild steel in 3% NaCl aerated solution, J. Mol. Liq. 250 (2018) 50–62.

[10] M.M. Solomon, H. Gerengi, S.A. Umoren, Carboxymethyl cellulose/silver nanoparticles composite: synthesis, characterization and application as a benign corrosion inhibitor for St37 steel in 15% H_2SO_4 medium, ACS Appl. Mater. Interfaces 9 (2017) 6376 − 6389.

[11] M.M. Solomon, H. Gerengi, T. Kaya, S.A. Umoren, Performance evaluation of a chitosan/silver nanoparticles composite on St37 steel corrosion in a 15% HCl solution, ACS Sustain. Chem. Eng. 5 (2017) 809 − 820.

[12] B.D.B. Tiu, R.C. Advincula, Polymeric corrosion inhibitors for the oil and gas industry: design principles and mechanism, React. Funct. Polym. 95 (2015) 25–45.

[13] E.E. Oguzie, Hydroxypropyl methylcellulose as a polymeric corrosion inhibitor for aluminium, Pigm. Resin Technol. 43 (2014) 151–158.

[14] M.M. Solomon, S.A. Umoren, I.I. Udosoro, A.P. Udoh, Inhibitive and adsorption behaviour of carboxymethyl cellulose on mild steel corrosion in sulphuric acid solution, Corros. Sci. 52 (2010) 1317–1325.

[15] C. Jeyaprabha, S. Sathiyanarayanan, G. Venkatachari, Effect of cerium ions on corrosion inhibition of PANI for iron in 0.5 M H2SO4, Appl. Surf. Sci. 253 (2006) 432–438.

[16] S. Sathiyanarayanan, C. Jeyaprabha, G. Venkatachari, Influence of metal cations on the inhibitive effect of polyaniline for iron in 0.5 M H_2SO_4, Mater. Chem. Phys. 107 (2008) 350–355.

[17] N. Manimaran, S. Rajendran, M. Manivannan, S. John Mary, Corrosion inhibition of carbon steel by polyacrylamide, Res. J. Chem. Sci. 2 (2012) 52–57.

[18] S.A. Umoren, M.M. Solomon, Synergistic corrosion inhibition effect of metal cations and mixtures of organic compounds: a review, J. Environ. Chem. Eng. 5 (2017) 246–273.

[19] P. Manivel, S. Sathiyanarayanan, G. Venkatachari, Influence of H^+ and Cl^- ions on inhibitive performance of poly(aniline) for iron corrosion in acid, J. Appl. Polym.

Sci. 106 (2007) 3988–3993.
[20] I.O. Arukalam, I.C. Madufor, O. Ogbobe, E.E. Oguzie, Hydroxypropyl methylcellulose as a polymeric corrosion inhibitor for aluminium, Pigm. Resin Technol. 43 (2014) 151–158.
[21] I.O. Arukalam, I.C. Madufor, O. Ogbobe, E.E. Oguzie, Experimental and theoretical studies of hydroxyethyl cellulose as inhibitor for acid corrosion inhibition of mild steel and aluminium, Open Corros. J. 6 (2014) 1–10.
[22] S.A. Umoren, M.M. Solomon, Effect of halide ions on the corrosion inhibition efficiency of different organic species – a review, J. Ind. Eng. Chem. 21 (2015) 81–100.
[23] M.M. Solomon, H. Gerengi, T. Kaya, E. Kaya, S.A. Umoren, Synergistic inhibition of St37 steel corrosion in 15% H_2SO_4 solution by chitosan and iodide ion additives, Cellulose 24 (2017) 931–950.
[24] M.M. Solomon, S.A. Umoren, Electrochemical and gravimetric measurements of inhibition of aluminum corrosion by poly (methacrylic acid) in H_2SO_4 solution and synergistic effect of iodide ions, Measurement 76 (2015) 104–116.
[25] H.T. Clarke, H.B. Gillespie, S.Z. Weishaus, The action of formaldehyde on amines and amino acids, J. Am. Chem. Soc. 55 (1933) 4571–4587.
[26] G.B. Butler, Cyclopolymerization and Cyclocopolymerization, Marcel Dekker, New York, 1992.
[27] Q. Tian, Z. Liu, Y. Zhu, X. Dong, Y. Saih, J.M. Basset, M. Sun, W. Xu, L. Zhu, D. Zhang, Beyond creation of mesoporosity: the advantages of polymer-based dual-function templates for fabricating hierarchical zeolites, Adv. Funct. Mater. 26 (2016) 1881–1891.
[28] ASTM-G 01–03, ASTM Book of Standards, vol. 3, ASTM, West Conshohocken, 2003, p. 02.
[29] ASTM-G 01–90, Standard practice for preparing, cleaning, and evaluation corrosion test specimens, ASTM Book of Standards, 1999 Reapproved.
[30] Y.Z. Li, N. Xu, X.P. Guo, G.A. Zhang, Inhibition effect of imidazoline inhibitor on the crevice corrosion of N80 carbon steel in the CO_2-saturated NaCl solution containing acetic acid, Corros. Sci. 126 (2017) 127–141.
[31] ASTM G3-89, Conventions applicable to electrochemical measurements in corrosion testing, Annual Book of ASTM Standard, vol. 30, 1994 Reapproved.
[32] ASTM G3-94, Making potentiostatic and potentiodynamic anodic polarization measurements, Annual Book of ASTM Standard 48, 1994 Reapproved.
[33] O. Kaczerewska, R. Leiva-Garcia, R. Akid, B. Brycki, I. Kowalczyk, T. Pospieszny, Effectiveness of O-bridged cationic gemini surfactants as corrosion inhibitors for stainless steel in 3 M HCl: experimental and theoretical studies, J. Mol. Liq. 249 (2018) 1113–1124.
[34] M. El Achouri, M.R. Infante, F. Izquierdo, S. Kertit, H.M. Gouttaya, B. Nciri, Synthesis of some cationic gemini surfactants and their inhibitive effect on iron corrosion in hydrochloric acid medium, Corros. Sci. 43 (2001) 19–35.
[35] S.A. Haladu, S.A. Umoren, S.A. Ali, M.M. Solomon, A.I. Mohammed, Synthesis, characterization and electrochemical evaluation of anticorrosion property of a tetrapolymer for carbon steel in strong acid media, Chin. J. Chem. Eng. (2018), https://doi.org/10.1016/j.cjche.2018.07.015.
[36] P. Han, C. Chen, W. Li, H. Yu, Y. Xu, L. Ma, Y. Zheng, Synergistic effect of mixing cationic and nonionic surfactants on corrosion inhibition of mild steel in HCl: experimental and theoretical investigations, J. Colloid Interface Sci. 516 (2018) 398–406.
[37] G. Sı˘gırcık, T. Tüken, M. Erbil, Assessment of the inhibition efficiency of 3,4-diaminobenzonitrile against the corrosion of steel, Corros. Sci. 102 (2016) 437–445.
[38] M.T. Alhaffar, S.A. Umoren, I.B. Obot, S.A. Ali, Isoxazolidine derivatives as corrosion inhibitors for low carbon steel in HCl solution: experimental, theoretical and effect of KI studies, RSC Adv. 8 (2018) 1764–1777.
[39] S. Pareek, D. Jain, S. Hussain, A. Biswas, R. Shrivastava, S.K. Parida, H.K. Kisan, H. Lgaz, I.-M. Chung, D. Behera, A new insight into corrosion inhibition mechanism of copper in aerated 3.5% (by weight) NaCl solution by eco-friendly imidazopyrimidine dye: experimental and theoretical approach, Chem. Eng. J. (2018), https://doi.org/10.1016/j.cej.2018.08.079.
[40] M. Outirite, M. Lagrenée, M. Lebrini, M. Traisnel, C. Jama, H. Vezin, F. Bentiss, Ac impedance, X-ray photoelectron spectroscopy and density functional theory studies of 3,5-bis(n-pyridyl)-1,2,4-oxadiazoles as efficient corrosion inhibitors for carbon steel surface in hydrochloric acid solution, Electrochim. Acta 55 (2010) 1670–1681.
[41] H. Ouicia, M. Tourabib, O. Benalic, C. Sellesd, C. Jamae, A. Zarroukf, F. Bentiss, Adsorption and corrosion inhibition properties of 5-amino 1,3,4-thiadiazole2-thiol on the mild steel in hydrochloric acid medium: thermodynamic, surface and electrochemical studies, J. Electroanal. Chem. 803 (2017) 125–134.
[42] K. Boumhara, M. Tabyaoui, C. Jama, F. Bentiss, Artemisia Mesatlantica essential oil as green inhibitor for carbon steel corrosion in 1 M HCl solution: electrochemical and XPS investigations, J. Ind. Eng. Chem. 29 (2015) 146–155.
[43] A. Farahi, F. Bentiss, C. Jama, M.A. El Mhammedi, M. Bakasse, A new approach in modifying ethylene glycol methacrylate phosphate coating formulation by adding sodium montmorillonite to increase corrosion resistance properties, J. Alloys Compd. 723 (2017) 1032–1038.
[44] A. Rauf, W.F. Bogaerts, Monitoring of crevice corrosion with the electrochemical frequency modulation technique, Electrochim. Acta 54 (2009) 7357–7363.
[45] A. Rauf, W.F. Bogaerts, Employing electrochemical frequency modulation for pitting corrosion, Corros. Sci. 52 (2010) 2773–2785.
[46] P. Beesea, H. Venzlaff, J. Srinivasan, J. Garrelfs, M. Stratmann, K.J.J. Mayrhofer, Monitoring of anaerobic microbially influenced corrosion via electrochemical frequency modulation, Electrochim. Acta 105 (2013) 239–247.
[47] I.B. Obot, I.B. Onyeachu, Electrochemical frequency modulation (EFM) technique: theory and recent practical applications in corrosion research, J. Mol. Liq. 249 (2018) 83–96.
[48] S.S. Abdel-Rehimb, K.F. Khaled, N.S. Abd-Elshafia, Electrochemical frequency modulation as a new technique for monitoring corrosion inhibition of iron in acid media by new thiourea derivative, Electrochim. Acta 51 (2006) 3269–3277.
[49] H.H. Zhang, Y. Chen, Experimental and theoretical studies of benzaldehyde thiosemicarbazone derivatives as corrosion inhibitors for mild steel in acid media, J. Mol. Struct. 1177 (2019) 90–100.
[50] C. Wang, J. Chen, J. Han, C. Wang, B. Hu, Enhanced corrosion inhibition performance of novel modified polyaspartic acid on carbon steel in HCl solution, J. Alloys Compd. 771 (2019) 736–746.
[51] M. Ramezanzadeh, G. Bahlakeh, Z. Sanaei, B. Ramezanzadeh, Corrosion inhibition of mild steel in 1M HCl solution by ethanolic extract of eco-friendly *Mangifera indica* (mango) leaves: electrochemical, molecular dynamics, Monte Carlo and ab initio study, Appl. Surf. Sci. 463 (2019) 1058–1077.
[52] M. Djenane, S. Chafaa, N. Chafai, R. Kerkour, A. Hellal, Synthesis, spectral properties and corrosion inhibition efficiency of new ethyl hydrogen [(methoxyphenyl) (methylamino) methyl] phosphonate derivatives: experimental and theoretical investigation, J. Mol. Struct. 1175 (2019) 398–413.
[53] Y.S. Papir, A.H. Schroeder, P.J. Stone, New downhole filming amine corrosion inhibitor for sweet and sour production, SPE 18489 Presented at the SPE International Symposium on Oilfield Chemistry in Houston, TX, February 8–10, 1989.
[54] A.Y. Musa, A.B. Mohamad, A.A.H. Kadhum, M.S. Takriff, L.T. Tien, Synergistic effect of potassium iodide with phthalazone on the corrosion inhibition of mild steel in 1.0 M HCl, Corros. Sci. 53 (2011) 3672–3677.
[55] N. C, alis, kan, S. Bilgic, Effect of iodide ions on the synergistic inhibition of the corrosion of manganese-14 steel in acidic media, Appl. Surf. Sci. 153 (2000) 128–133.
[56] B. Qian, J. Wang, M. Zheng, B. Hou, Synergistic effect of polyaspartic acid and iodide ion on corrosion inhibition of mild steel in H_2SO_4, Corros. Sci. 75 (2013) 184–192.
[57] S.A. Umoren, M.M. Solomon, U.M. Eduok, I.B. Obot, A.U. Israel, Inhibition of mild steel corrosion in H_2SO_4 solution by coconut coir dust extract obtained from different solvent systems and synergistic effect of iodide ions: ethanol and acetone extracts, J. Environ. Chem. Eng. 2 (2014) 1056.
[58] Z.B. Wang, H.X. Hu, Y.G. Zheng, W. Ke, Y.X. Qiao, Comparison of the corrosion behavior of pure titanium and its alloys in fluoride-containing sulfuric acid, Corros. Sci. 103 (2016) 50–65.
[59] Z.B. Wang, H.X. Hu, Y.G. Zheng, Synergistic effects of fluoride and chloride on general corrosion behavior of AISI 316 stainless steel and pure titanium in H_2SO_4 solutions, Corros. Sci. 130 (2018) 203–217.
[60] M.M. Solomon, S.A. Umoren, I.B. Obot, A.A. Sorour, H. Gerengi, Exploration of dextran for application as corrosion inhibitor for steel in strong acid environment: effect of molecular weight, modification, and temperature on efficiency, ACS Appl. Mater. Interfaces 10 (2018) (28112 − 28129).
[61] E.A. Norr, The inhibition of mild steel corrosion in phosphoric acid by some N-heterocyclic compounds in the salt form, Corros. Sci. 47 (2005) 33.
[62] S.A. Umoren, Polypropylene glycol: a novel corrosion inhibitor for ×60 pipeline steel in 15% HCl solution, J. Mol. Liq. 219 (2016) 946–958.
[63] A. Popova, M. Christov, A. Vasilev, Mono- and dicationic benzothiazolic quaternary ammonium bromides as mild steel corrosion inhibitors. Part III: influence of the temperature on the inhibition process, Corros. Sci. 94 (2015) 70–78.
[64] M.M. Solomon, S.A. Umoren, A.U. Israel, E.E. Ebenso, Polypropylene glycol-silver nanoparticle composites: a novel anticorrosion material for aluminum in acid medium, J. Mater. Eng. Perform. 24 (2015) 4213.
[65] M.M. Solomon, S.A. Umoren, In-situ preparation, characterization and anticorrosion property of polypropylene glycol/silver nanoparticles composite for mild steel corrosion in acid solution, J. Colloid Interface Sci. 462 (2016) 29–41.
[66] X. Ma, X. Jiang, S. Xia, M. Shan, X. Li, L. Yu, Q. Tang, New corrosion inhibitor acrylamide methyl ether for mild steel in 1 M HCl, Appl. Surf. Sci. 371 (2016) 248–257.
[67] A. Yurt, A. Balaban, S.U. Kandemir, G. Bereket, B. Erk, Investigation on some Schiff bases as HCl corrosion inhibitors for carbon steel, Mater. Chem. Phys. 85 (2004) 420–426.
[68] Mitutoyo Corporation, Surface Finish Analysis, (2014), pp. 1–58 https://www.mitutoyo.com/wp-content/uploads/2012/1984_Surf_Roughness_PG.pdf.
[69] EN ISO 4287, Geometrical Product Specifications (GPS) − Surface Texture: Profile Methods − Terms, Definitions, and Surface Parameters, (1998).
[70] M.A.J. Mazumder, H.A. Al-Muallem, A.A. Ali, The effects of N-pendants and electron-rich amidinemotifsin 2-(p-alkoxyphenyl)-2-imidazolines on mild steel corrosion in CO2-saturated 0.5 M NaCl, Corros. Sci. 90 (2015) 54–68.
[71] O.A. de Oliveira, O.V. Correa, D.J. dos Santos, A.A. Zúñiga Páez, A.C. Lopes de Oliveira, R.A. Antunes, Effect of silicate-based films on the corrosion behavior of the API 5L X80 pipeline steel, Corros. Sci. 139 (2018) 21 − 34.
[72] N.D. Nam, Q.V. Bui, M. Mathesh, M.Y.J. Tan, M. Forsyth, A study of 4-carboxyphenylboronic acid as a corrosion inhibitor for steel in carbon dioxide containing environments, Corros. Sci. 76 (2013) 257–266.
[73] N.D. Nam, A. Somers, M. Mathesh, M. Seter, B. Hinton, M. Forsyth, M.Y.J. Tan, The behaviour of praseodymium 4-hydroxycinnamate as an inhibitor for carbon dioxide corrosion and oxygen corrosion of steel in NaCl solutions, Corros. Sci. 80 (2014) 128–138.
[74] Y. Tang, X.P. Guo, G.A. Zhang, Corrosion behaviour of X65 carbon steel in supercritical-CO_2 containing H_2O and O_2 in carbon capture and storage (CCS) technology, Corros. Sci. 118 (2017) 118–128.
[75] M.M. Solomon, H. Gerengi, S.A. Umoren, N.B. Essien, U.B. Essien, E. Kaya, Gum Arabic-silver nanoparticles composite as a green anticorrosive formulation for steel corrosion in strong acid media, Carbohydr. Polym. 181 (2018) 43–55.
[76] M. Descostes, F. Mercier, N. Thromat, C. Beaucaire, M. Gautier-Soyer, Use of XPS in the determination of chemical environment and oxidation state of iron and sulfur

samples: constitution of a data basis in binding energies for Fe and S reference compounds and applications to the evidence of surface species of an oxidized pyrite in a carbonate medium, Appl. Surf. Sci. 165 (2000) 288 − 302.

[77] A. Zarrouk, B. Hammouti, T. Lakhlifi, M. Traisnel, H. Vezin, F. Bentiss, New 1H-pyrrole-2,5-dione derivatives as efficient organic inhibitors of carbon steel corrosion in hydrochloric acid medium: electrochemical, XPS and DFT studies, Corros. Sci. 90 (2015) 572–584.

[78] U. Eduok, E. Ohaeri, J. Szpunar, Electrochemical and surface analyses of X70 steel corrosion in simulated acid pickling medium: effect of poly (N-vinyl imidazole) grafted carboxymethyl chitosan additive, Electrochim. Acta 278 (2018) 302 − 312.

[79] G. Kalita, K. Wakita, M. Takahashi, M. Umeno. Iodine doping in solid precursor-based CVD growth graphene film. J. Mater. Chem. 21 (2011) 15209–15213.